Dust in the Early Universe : Dust Formation in the Ejecta of Population III Supernovae

Takaya Nozawa and Takashi Kozasa

Division of Earth and Planetary Sciences, Graduate School of Science, Hokkaido University, Sapporo 060-0810, Japan; nozawabozo@ep.sci.hokudai.ac.jp, kozasa@ep.sci.hokudai.ac.jp

and

Hideyuki Umeda, Keiichi Maeda, and Ken'ichi Nomoto

Department of Astronomy, School of Science, University of Tokyo, Bunkyo-ku, Tokyo 113-0033, Japan; umeda@astron.s.u-tokyo.ac.jp, maeda@astron.s.u-tokyo.ac.jp, nomoto@astron.s.u-tokyo.ac.jp

ABSTRACT

Dust grains play a crucial role on formation and evolution history of stars and galaxies in the early universe. We investigate the formation of dust grains in the ejecta of population III supernovae including pair–instability supernovae which are expected to occur in the early universe, applying a theory of non–steady state nucleation and grain growth. Dust formation calculations are performed for core collapse supernovae with the progenitor mass M_{pr} ranging from 13 to 30 $M_\odot$ and for pair–instability supernovae with $M_{pr} = 170$ and 200 $M_\odot$. In the calculations, the time evolution of gas temperature in the ejecta, which strongly affects the number density and size of newly formed grains, is calculated by solving the radiative transfer equation taking account of the energy deposition of radio active elements. Two extreme cases are considered for the elemental composition in the ejecta; unmixed and uniformly mixed cases within the He–core, and formation of CO and SiO molecules is assumed to be complete.

The results of calculations for core collapse supernovae and pair–instability supernovae are summarized as the followings; in the unmixed ejecta, a variety of grain species condense, reflecting the difference of the elemental composition at the formation site in the ejecta, otherwise only oxide grains condense in the uniformly mixed ejecta. The average size of newly formed grains spans the range

of three orders of magnitude, depending on the grain species and the formation condition, and the maximum radius is limited to less than 1 μm, which does not depend on the progenitor mass. The size distribution function of each grain species is approximately log–normal, except for Mg–silicates, MgO, Si and FeS grains in the unmixed case and Al_2O_3 grain in the both cases. The size distribution function summed up over all grain species is approximated by a power–law formula whose index is -3.5 for the larger radius and -2.5 for the smaller one; the radius at the crossover point ranges from 0.004 to 0.1 μm, depending on the model of supernovae. The fraction of mass locked into dust grains increases with increasing the progenitor mass; 2–5 % of the progenitor mass for core collapse supernovae and 15–30 % for pair–instability supernovae whose progenitor mass ranges from 140 to 260 $M_\odot$. Thus, if the very massive stars populate the first generation stars (population III stars), a large amount of dust grains would be produced in the early universe. We also discuss the dependence of the explosion energy and the amount of ^{56}Ni in the ejecta as well as the efficiency of formation of CO and SiO molecules on the formation of dust grains in the ejecta of supernovae.

Subject headings: dust: formation—supernovae: general—supernovae: population III

1. Introduction

The recent observations of the reddening of background quasars and the damped Lyα systems in the spectra of distant quasars have confirmed the presence of dust grains at high–redshifted universe (e.g., Pettini et al. 1994, 1997; Pei & Fall 1995). Dust grains play a critical role on formation and evolution history of stars and galaxies in the early universe: Dust grains absorb stellar light and re–emit it by thermal radiation, which controls the energy balance in the interstellar space and the evolution of gas clouds. Also the surface of dust grains is an efficient site for formation of H_2 molecules which act as an effective coolant at the time of formation of stars from interstellar clouds, and enhance the star formation rate (SFR) and strongly affect the initial mass function (IMF) in the metal–poor universe (Hirashita, Hunt, & Ferrara 2002; Hirashita & Ferrara 2002). In fact, the most iron–poor star HE0107–5240 so far discovered (Christlieb et al. 2002) has raised important questions on the formation of such a metal–poor ([Fe/H]=-5.3 ± 0.2) but low–mass ($\sim 0.8\ M_\odot$) star. Umeda & Nomoto (2003a) showed that this star can be the second generation star formed from a gas cloud enriched by a population III supernova, which produced very little Fe but

large enough C and O for efficient gas cooling. Schneider et al. (2003) also considered this star as the second generation but argued the dust grains produced by population III objects could play an important role in forming low mass stars from such a metal–poor gas cloud as [Fe/H]$=-5.1$. Furthermore, dust grains residing in interstellar space in galaxies and in intergalactic medium cause obscuration and reddening of starlight, and the thermal radiation from the dust grains distorts the cosmic background radiation (see Hauser & Dwek 2001 for details). How much dust grains absorb stellar light and re–emit it by thermal radiation heavily depends on their chemical composition, size and abundance. Therefore, the investigation of dust grains in the early universe is inevitable not only to reveal the structure and evolution of the early universe but also to deduce the SFR and the IMF during the evolution of the universe from the observations of the cosmic microwave background (CMB) and the cosmic infrared background (CIB) which could be one of the main subjects of the planned Atacama Large Millimeter Array (ALMA) and the Next Generation Space Telescope (NGST) (Loeb & Haiman 1997).

In cosmic environments, dust grains form in a cooling gas outflowing from star to interstellar space such as in the stellar winds from AGB stars and in the ejecta of supernovae. The major source of dust grains in our Galaxy is considered to be AGB stars evolving from stars with main–sequence mass $\leq 8\ M_\odot$. However, the age of AGB stars is too old to contribute to dust grains in the early universe. Thus, supernovae evolving from stars whose main–sequence mass is larger than $8\ M_\odot$ are considered to be the major source of dust grains in the early universe. Dust formation in the ejecta of supernovae has been suggested from the isotopic anomalies in meteorites, and the microscopic analysis of each dust grains extracted from meteorites has identified SiC, graphite and Si_3N_4 grains as the supernovae condensates (SUNOCONs) from their isotopic composition (see Zinner 1998 for details). SN 1987A is the first supernova in which the in–situ dust formation in the expanding ejecta was observed (Lucy et al. 1989; Whitelock et al. 1989; Meikle et al. 1993; Wooden et al. 1993; Colgan et al. 1994), and the model of formation of dust grains in the ejecta was investigated by Kozasa, Hasegawa, & Nomoto (1989a,b, 1991). Also the dust formation was confirmed in the ejecta of SN 1999em from the appearance of blue–shifted line emissions as observed in SN 1987A (Elmhamdi et al. 2003).

What kind of and how much dust grains condense in the ejecta have been still on debate. The observations of young supernova remnants (SNRs) with Infrared Space Observatory (ISO) revealed the thermal radiation from dust grains condensed in the ejecta of Cas A (Lagage et al. 1996; Arendt, Dwek, & Moseley 1999), and the observed thermal radiation is well fitted by a mixture of Al_2O_3, $MgSiO_3$ and SiO_2 grains (Douvion, Lagage, & Pantin 2001), otherwise the spectroscopic observation at 2.4–45 μm suggested that the pristine dust in Cas A is a peculiar class of silicate material (Arendt, Dwek, & Moseley 1999). However,

no thermal radiation originating from dust grains formed in the ejecta was observed towards the Tycho, Kepler and Crab SNRs by ISO (Douvion et al. 2001), despite that the optical observations have suggested the presence of dust grains in the Crab SNR (Fesen & Blair 1990; Hester et al. 1990). The estimated amount of hot dust observed in Cas A SNR by ISO (Arendt, Dwek, & Moseley 1999) is 10 to 100 times smaller than the previous value estimated from IRAS observations (e.g., Mezger et al. 1986; Dwek et al. 1987). However the recent submillimeter observations by SCUBA have revealed the existence of cold dust in the young SNR of Cas A and concluded that the amount of dust condensed in the ejecta is estimated to reach a few $M_\odot$ (Dunne et al. 2003). These observations strongly support that Type II supernovae could be the major source of dust grains in the early universe.

Of course, the chemical composition, size and amount of dust grains in the early universe are determined by the balance between production in the ejecta of supernovae and destruction by interstellar shock as well as reverse shock penetrating into the ejecta (see, e.g., Dwek 1998 for details), and the investigation of dust formation in the ejecta of population III supernovae is the first step to reveal the nature of dust grains in the early universe. Todini & Ferrara (2001) performed the dust formation calculations in the primordial core collapse supernovae with the progenitor mass $M_{\rm pr}$ ranging from 12 to 35 $M_\odot$, adopting the models of supernovae by Woosley & Weaver (1995) and applying the method of dust formation calculation for SN 1987A by Kozasa, Hasegawa, & Nomoto (1989a, 1991) as a template. In the calculations, they considered one–zone model for elemental composition and density in the ejecta, assuming the uniform mixing of elements within the He–core. Taking account of formation and destruction of CO and SiO molecules, they showed that carbon grain condenses first and then Al_2O_3, Mg–silicates and Fe_3O_4 grains condense in this order as the gas cools down. Also, they showed that the size of newly formed grains is relatively small ($\leq$ 300 Å in radius) and is sensitive to the value of adiabatic index γ, and that the total mass of produced dust is about 0.08 to 0.3 $M_\odot$ per supernova.

The recent theoretical investigations of fragmentation of gas clouds in the metal–free early universe have claimed that the stars more massive than some tens–100 $M_\odot$ populate the first generation stars (Nakamura & Umemura 2001; Bromm, Coppi, & Larson 2002). Such metal–free stars massive as 140 $M_\odot \leq M_{\rm pr} \leq 260$ $M_\odot$ may evolve stably to end up their lives as pair–instability supernovae (e.g., Umeda & Nomoto 2002; Heger & Woosley 2002). Also Umeda & Nomoto (2002) have suggested that hypernovae whose explosion energy is more than several to ten times that of the ordinary core collapse supernovae are necessary to reproduce the enhancement of Zn and iron–peak elements observed in metal–poor stars. Therefore, in this paper, we explore the dust formation in the ejecta of population III supernovae including hypernovae and pair–instability supernovae to investigate the dependence of the progenitor mass and the explosion energy on the formation of dust grains in the ejecta.

Our main aim is to clarify the dependence of the yield of newly formed grains and their size on the progenitor mass, focusing on the ordinary core collapse supernovae and pair–instability supernovae. We also investigate the effects of the explosion energy and the mass of ^{56}Ni in the ejecta as well as the efficiency of formation of CO and SiO molecules on the formation of dust grains.

As discussed by Kozasa, Hasegawa, & Nomoto (1989a), the elemental composition in the ejecta controls what kind of grain species condenses, and the temporal evolution of gas density and temperature in the ejecta strongly affects the size of newly formed grains in the ejecta. Thus, in the dust formation calculations we employ the hydrodynamical models and the elemental compositions of population III supernovae calculated by Umeda & Nomoto (2002). The time evolution of gas temperature is calculated by the multifrequency radiative transfer code taking account of the energy deposition from radio active elements (Iwamoto et al. 2000). The two extreme cases for the elemental composition in the ejecta are considered; the elemental composition with original onion–like structure (hereafter referred to as unmixed case) and the uniformly mixed case within the He–core. A theory of non–steady state nucleation and grain growth is applied for the calculation of dust grains under the assumption that formation of CO and SiO molecules is complete. Formation of all possible condensates is taken into account simultaneously to clarify what kind of grain species really condenses.

In section 2 we present the models of supernovae used in the calculations, and the method of dust formation calculation is described in section 3. The results of calculations for ordinary core collapse supernovae and pair–instability supernovae are presented and discussed in section 4, and summarized in section 5. The effects of the explosion energy and the amount of ^{56}Ni in the ejecta as well as the efficiency of formation of CO and SiO molecules on the dust formation in the ejecta of supernovae are presented in Appendix A and B, respectively.

2. Model of the population III supernovae

The nature of population III supernovae has been extensively investigated to decipher the chemical evolution of the early universe compared with the observed elemental abundance of metal–poor stars (Umeda & Nomoto 2002, 2003b). Umeda & Nomoto (2002) have suggested that, in addition to ordinary core collapse supernovae with the explosion energy $\sim$ 10^{51} erg, hypernovae whose explosion energy is larger than 5–50×10^{51} erg (e.g., Nomoto et al. 2001, 2003 for reviews) are necessary to reproduce the enhancement of Zn and iron–peak elements observed in metal–poor stars. Also in the metal–free universe very massive stars

with mass ranging from 140 to 260 $M_\odot$ evolve stably and explode as the pair–instability supernovae for which the star is completely disrupted by nuclear–powered explosion (Umeda & Nomoto 2002; Heger & Woosley 2002).

We apply the hydrodynamical models and the results of nucleosynthesis calculations of population III supernovae by Umeda & Nomoto (2002) for the dust formation calculations. The details of the model used in the present calculations are summarized in Table 1, where the labels C, P and H of the model represent ordinary core collapse supernovae (CCSNe), pair–instability supernovae (PISNe) and hypernovae (HNe), respectively, and the numerical value denotes the mass of progenitor in units of solar mass. The mass cut is the mass coordinate of the boundary between the ejecta and the remnant, and its value specifies the mass of ^{56}Ni in the ejecta; $M(^{56}\text{Ni}) = 0.07\ M_\odot$ is taken as a typical value for ordinary CCSNe to reproduce the observed behavior of early light curve for CCSNe. The models of HNe (H20A, B and H30A, B) are adopted to investigate the dependence of the explosion energy and the mass of ^{56}Ni in the ejecta on dust formation. The elemental composition and the temporal evolution of gas density and temperature in the ejecta, which are essential to investigate the dust formation, are summarized in the following subsections.

2.1.   Elemental composition

The elemental composition in the ejecta determines what kind of grain species condenses. No dust grain condenses in the hydrogen envelope of population III supernovae because the hydrogen envelope is metal–free. Even if heavy elements are intruded into the hydrogen envelope during the evolution of progenitor, the low density and the high expansion velocity prevent dust grains from condensing in the hydrogen envelope as discussed by Kozasa, Hasegawa, & Nomoto (1989a, 1991). Thus, the dust formation region in the ejecta of population III supernovae is confined within the He–core where heavy elements exist.

Figure 1 shows the elemental composition within the unmixed He–core at day 600 after the explosion, taking account of the decay of radio active elements; Fig. 1a for a model of CCSNe (C20) and Fig. 1b for PISNe (P170). The ejecta is divided into five regimes according to the elemental composition of interest to dust formation; for example, in the ejecta of the model C20, Fe–Si–S layer ($2.45\ M_\odot \le M_r \le 2.52\ M_\odot$), Si–S–Fe layer ($2.52\ M_\odot \le M_r \le 2.95\ M_\odot$), O–Si–Mg layer ($2.95\ M_\odot \le M_r \le 3.14\ M_\odot$), O–Mg–Si layer ($3.14\ M_\odot \le M_r \le 4.92\ M_\odot$) and He–layer ($4.92\ M_\odot \le M_r \le 5.79\ M_\odot$).

The He–layer is carbon–rich (C/O > 1) for CCSNe and its mass irregularly varies with the progenitor mass in the models of CCSNe used in this paper. The mass of oxygen–rich

layer (O–Si–Mg layer and O–Mg–Si layer) increases with increasing the progenitor mass, and the mass of inner Si–S–Fe and Fe–Si–S layer depends on the value of the mass cut. On the other hand, in the ejecta of PISNe, the He–layer is very thin for P170 and the mass increases with increasing the progenitor mass.

The mixing of elements in the ejecta of SN 1987A was confirmed from the early emergence of X–rays and γ–rays (e.g., Dotani et al. 1987; Itoh et al. 1987; Kumagai et al. 1988), and also the hydrodynamical simulations (Hachisu et al. 1990; see Arnett et al. 1989 for a review and references) and the laboratory experiments (Drake et al. 2002) clearly demonstrate that the mixing of elements is caused by the Rayleigh–Taylor instability at the interface of each layer with the different elemental composition. The isotopic signatures in the presolar carbon and SiC grains identified as SUNOCONs have suggested the extensive and microscopic mixing of elements in the different layers in the explosion (Amari & Zinner 1997; Travaglio et al. 1999). Thus, as an ideal case, the uniform mixing of elements within the He–core was considered to investigate dust formation in the ejecta of supernovae (Kozasa, Hasegawa & Nomoto 1989a; Todini & Ferrara 2001; Schneider, Ferrara, & Salvaterra 2003). On the other hand, Douvion, Lagage, & Pantin (2001) have suggested that the mixing in the ejecta of the Cas A SNR is knotty rather than microscopic. A simple calculation of molecular diffusion has shown that the mixing at atomic level is impossible before the condensation of dust grains in the ejecta (Deneault, Clayton, & Heger 2003). It has been still on debate at this moment whether the mixing is macroscopic at knotty level or microscopic at atomic level and how large the mixing is extended in the ejecta. Therefore, in the following calculation of dust formation we consider the two extreme cases for the mixing of elements; one is the unmixed case with the original onion–like structure, and another is the mixed case for which the elements are uniformly mixed within the He–core.

2.2. The time evolution of gas density and temperature in the ejecta

The time evolution of gas density and temperature strongly affects the number density and size of newly formed grains in the ejecta. As the explosion shock propagates outwards, the reverse shock generated at the interface of layers with different chemical composition changes the density structure. Although Deneault, Clayton, & Heger (2003) show that the reverse shock generated at the He–H interface introduces a very nonhomologous readjustment after $t = 10^6$ seconds from the explosion, our hydrodynamical calculations including the interaction with the reverse shock have shown that the interaction makes the expansion finally homologous in less than one day after the explosion (see Shigeyama & Nomoto 1990).

Thus, the time evolution of gas density at a given mass coordinate M_r is calculated by

$$\rho(M_r, t) = \rho(M_r, t_0) \left(\frac{t}{t_0} \right)^{-3} \tag{1}$$

where the reference time t_0 is one day after the explosion. The distribution of gas density within the He–core at day 600 after the explosion is shown in Figure 2 where the mass coordinate is normalized to the He–core mass and the histogram presentation of the density structure reflects the size of mesh used in the calculations: Fig. 2a for CCSNe (C20 and C25) and HNe (H25), and Fig. 2b for PISNe (P170 and P200). The gas density within the He–core of CCSNe with the same explosion energy is almost the same in the order of magnitude and does not depend so much on the progenitor mass, apart from the detailed structure caused by the propagation of reverse shock originating at the interface of each layer. The gas density in the ejecta of H25 is one order of magnitude lower than that of CCSNe, reflecting the explosion energy of ten times of CCSNe. Also the gas density in the ejecta of P200 is a little bit lower than that in the ejecta of P170, but the gas density within the He–core is 10^{-14}–10^{-13} g cm^{-3} at day 600 after the explosion and is almost the same order of the magnitude as the gas density in the ejecta of CCSNe, except for the region $M_r \leq 40\ M_\odot$.

The gas temperature in the ejecta is determined by the detailed process of the degradation of γ–rays and X–rays deposited from the radio active elements. In the previous calculations (Kozasa, Hasegawa, & Nomoto 1989a, 1991; Todini & Ferrara 2001), the time evolution of gas temperature was approximated by

$$T(M_r, t) = T(M_r, t_0) \left(\frac{t}{t_0} \right)^{3(1-\gamma)} \tag{2}$$

with a parameter γ, and the reference temperature $T(M_r, t_0)$ was determined by the observations of SN 1987A. However this method is not applicable for population III supernovae with no observational data. Therefore, the time evolution of gas temperature is calculated by using the multifrequency radiative transfer code together with the energy equation, taking account of the deposition of energy from radio active elements (see Iwamoto et al. 2000 for details).

As an example, Figs. 3a and 3b show the time evolution of gas temperature at a location of oxygen–rich layer with almost the same elemental composition in the ejecta of CCSNe, PISNe and HNe; Fig. 3a for the unmixed ejecta of C20 (at $M_r = 3.7\ M_\odot$), C25 (at $M_r = 4.6\ M_\odot$), P170 (at $M_r = 56.5\ M_\odot$) and P200 (at $M_r = 64.9\ M_\odot$), and Fig. 3b for the mixed ejecta of C25 (at $M_r = 4.6\ M_\odot$) and P200 (at $M_r = 64.9\ M_\odot$) and for the unmixed ejecta of H30A (at $M_r = 6.8\ M_\odot$) and H30B (at $M_r = 6.8\ M_\odot$). As can be seen from Figure 3,

it should be pointed out here that the temporal evolution of gas temperature in the ejecta is approximately determined only by the explosion energy and the amount of ^{56}Ni in the ejecta and does not heavily depend on the progenitor mass in the mass range considered in this paper. Also the gas temperature in the mixed ejecta is almost the same as that in the unmixed ejecta, except for the gas temperature around the day 200 after the explosion. The gas temperature in the ejecta of H30 with the large explosion energy quickly decreases in comparison with CCSNe, because X–rays and γ–rays escape easily due to the low gas density in the ejecta. The effect of $M(^{56}$Ni$)$ in the ejecta on the gas temperature is clearly shown by the difference of the gas temperature in the unmixed ejecta between H30A and H30B. The gas temperature in the ejecta of PISNe with the large explosion energy is much higher than that in CCSNe because the progenitor is massive and a large amount of ^{56}Ni reside in the ejecta.

From Figures 2 and 3, we can easily estimate the condensation time and the behavior of the average radius of a grain species formed in the ejecta of population III supernovae; if the grains condense around gas temperature of 1500 K in the oxygen–rich layer, the condensation time t_c after the explosion would be around day 400 for CCSNe, day 600 for PISNe and day 200 for HNe with the same $M(^{56}$Ni$)$ as CCSNe. The average radius of the condensate would be not so much different since the average size is roughly proportional to $\rho^{1/3} \propto (1/t_c)$, so far as the abundance of the elements available for dust formation is the same, which is confirmed by the results of dust formation calculations given in section 4 and Appendix A. Note that the radiation transfer calculation does not include the radiative cooling of molecules such as CO and SiO which act as effective coolants of gas in the ejecta as demonstrated by Liu & Dalgarno (1995) for SN 1987A. The effect of radiative cooling of molecules would make the condensation time of dust grains earlier and the average radius larger than those presented in section 4. However the average size and the number density of newly formed grains could not be so much different so far as the condensation time is in the order of one hundred days.

3.   Formulation and calculation of dust formation

3.1.   Formulation of nucleation and grain growth

In astrophysical environments, dust grains condense via formation of condensation nuclei and their growth through the collisions of gaseous species in a cooling gas outflowing from star into interstellar space.

The nucleation rate is usually formulated under the condition of presence of monomer molecule whose chemical composition is the same as the condensate. However, for formation

of compound grains of astrophysical interest such as silicates, no gaseous monomer molecule exists and it is impossible to derive rigorously the nucleation rate without specifying the chemical passways and reaction constants. Nevertheless, even if no information on chemical passways and reaction constants is available for formation of compound grains, as is discussed by Yamamoto et al. (2001), the nucleation rate can be evaluated by applying the concept of the key species introduced by Kozasa & Hasegawa (1987) when the net reaction rate is much larger than the decay rate. Under the assumption that the key species defined as the gaseous species of the least collision frequency among the reactants controls the kinetics of nucleation and grain growth, the steady state nucleation rate of j–th grain species $J_j^s(t)$ is given by

$$J_j^s(t) = \alpha_{sj} \Omega_j \left(\frac{2\sigma_j}{\pi m_{1j}} \right)^{1/2} \left(\frac{T}{T_d} \right)^{1/2} \Pi_j c_{1j} \exp\left[-\frac{4}{27} \frac{\mu_j^3}{(\ln S_j)^2} \right] \tag{3}$$

where α_{sj} is the sticking probability of the key species for j–th grain species, Ω_j is the volume of the condensate per the key species, and σ_j is the surface energy. We assume $\alpha_{sj} = 1$ in the calculations (see Hasegawa & Kozasa 1988; Kozasa et al. 1996; Chigai, Yamamoto, & Kozasa 1999 for the derivation of steady–state nucleation rate). The concentration and the mass of the key species for j–th grain species are denoted by c_{1j} and m_{1j}, respectively. T_d is the temperature of the condensation nuclei and T is the gas temperature (see Kozasa et al. 1996). The factor Π_j is a function of partial gas pressures of reactants and products except for the key species (Yamamoto et al. 2001) and we put $\Pi_j = 1$ in the calculations, partly because the appearance of the factor is somehow related with the detailed chemical reaction mechanism at the condensation and partly because the factor can be negligible under the condition that the number of the key species contained in the condensation nuclei is much larger than unity. The quantity μ_j representing the energy barrier for nucleation is defined by $\mu_j = 4\pi a_{0j}^2 \sigma_j / k T_d$ with the hypothetical radius of condensate per the key species $a_{0j} = (3\Omega_j/4\pi)^{1/3}$, where k is the Boltzmann constant. We assume the temperature of the condensation nuclei is the same as the gas temperature in what follows. The supersaturation ratio S_j taking into account the chemical reaction at the condensation of j–th grain species is calculated by

$$\ln S_j = -\frac{\Delta G_j^0}{kT} + \sum_i \nu_{ij} \ln P_{ij} \tag{4}$$

where the ΔG_j^0 is the Gibbs free energy of formation of j–th grain species from the reactants per the key species and P_{ij} are the partial gas pressures of reactant and product gas species. The stoichiometric coefficients ν_{ij} of reactants and products are normalized to the key species; ν_{ij} is positive for a reactant and negative for a product (see Kozasa & Hasegawa 1987; Hasegawa & Kozasa 1988).

In the ejecta of supernovae where the gas cooling time and/or the collision time controlling the process of nucleation and grain growth are comparable to the dynamical time scale, the application of the steady state nucleation rate is questionable. In this paper, according to Gail, Keller, & Sedlmayr (1984), we employ the non–steady state nucleation rate $J_j(t)$ evaluated by the equation

$$\frac{\partial}{\partial t}\left(\frac{J_j(t)}{\eta_j}\right) = -\frac{1}{\tau_{*,j}\eta_j}\left[J_j(t) - J_j^s(t)\right] \tag{5}$$

with the relaxation time towards the steady state $\tau_{*,j}$ defined by

$$\tau_{*,j}^{-1} = 4\pi a_{0j}^2 \alpha_{sj}\left(\frac{kT}{2\pi m_{1j}}\right)^{1/2} c_{1j}(t)\frac{(\ln S_j)^2}{\mu_j} = \tau_{\mathrm{coll},j}^{-1}\frac{(\ln S_j)^2}{\mu_j} \tag{6}$$

and $\eta_j = \tau_{\mathrm{coll},j}^{-1}(r_{c,j}/a_{0j})^2$, where $\tau_{\mathrm{coll},j}$ is the collision time of the key species and $r_{c,j} = 2a_{0j}\mu_j/3\ln S_j$ is the critical radius for j–th grain species.

Given the nucleation rate $J_j(t)$ at a time t, the process of nucleation and grain growth is described by the two basic equations in a frame comoving with gas; one is the equation of continuity for the key species given by

$$1 - \frac{c_{1j}(t)}{\tilde{c}_{1j}(t)} = 1 - Y_{1j} = \int_{t_e}^{t} \frac{J_j(t')}{\tilde{c}_{1j}(t')}\frac{4\pi}{3\Omega_j}r_j^3(t,t')dt', \tag{7}$$

where t_e is the equilibrium time defined as a time at which the supersaturation ratio S_j reaches to unity without depletion of the key species, and $\tilde{c}_{1j}$ is the nominal concentration of the key species expected without depletion of the key species due to nucleation and grain growth, and $Y_{1j} = c_{1j}/\tilde{c}_{1j}$ represents the degree of depletion of the key species due to nucleation and grain growth, and $r_j(t,t')$ is the radius of grain nucleated at t' and measured at t. Another is the equation of grain growth given by

$$\frac{dr_j}{dt} = \alpha_{sj}\Omega_j\left(\frac{kT}{2\pi m_{1j}}\right)^{1/2}c_{1j}(t) = \frac{1}{3}a_{0j}\tau_{\mathrm{coll},j}^{-1}(t). \tag{8}$$

By differentiating the equation (7) with t subsequently, the integral equation is reduced to the simultaneous ordinary equations

$$\frac{dK_j^{(i)}}{dt} = \frac{J_j(t)}{\tilde{c}_{1j}(t)}\frac{4\pi}{3\Omega_j}r_{c,j}^i + iK_j^{(i-1)}\frac{dr_j}{dt} \quad (\text{for } i = 1 - 3) \tag{9}$$

with

$$\frac{dK_j^{(0)}}{dt} = \frac{J_j(t)}{\tilde{c}_{1j}(t)}\frac{4\pi}{3\Omega_j}. \tag{10}$$

In principle, by solving the equations (5), (8), (9) and (10) in couple with the temporal evolution of gas density $\rho(t)$ and temperature $T(t)$ with the number abundances of reactants, the number density $n_{\mathrm{gr},j}(t)$ and volume equivalent average radius $r_{\mathrm{gr},j}(t)$ of j–th grain species are calculated by

$$\frac{n_{\mathrm{gr},j}}{\tilde{c}_{1j}(t)} = \frac{K_j^{(0)}(t)}{a_{0j}^3} \tag{11}$$

and

$$r_{\mathrm{gr},j}^3 = \frac{K_j^{(3)}(t)}{K_j^{(0)}(t)}, \tag{12}$$

respectively. Furthermore, the size distribution function $f_j(r)$ of newly formed j–th grain species at a time t is calculated by

$$f_j(r)dr = \frac{\tilde{c}_{1j}(t)}{a_{0j}^3}\frac{dK_j^{(0)}(t')}{dt'}dt' \tag{13}$$

since the grains with radii between r and $r + dr$ are nucleated in the time interval of t' and $t' + dt'$.

3.2. Calculation of dust formation in the ejecta of supernovae

Formation of dust grains in the ejecta of supernovae is calculated by solving the equations (5), (8), (9) and (10) with the temporal evolution of gas density and temperature, given the grain species and the chemical reaction at the condensation with the abundance of the reactants. The formation of CO and SiO molecules prior to the formation of dust grains was observed in the ejecta of SN 1987A (e.g., Bouchet & Danziger 1993). Formation of CO and SiO molecules plays a crucial role on the formation of dust grains, because CO molecules lock the oxygen atoms available for formation of oxide grains and SiO molecules are considered to be the starting molecules to form silicate grains.

As discussed by Liu & Dalgarno (1994, 1996), in the ejecta of supernovae, these molecules are destroyed by the impact with energetic electrons and charge transfer reactions with the ionized inert gaseous atoms which are created by the decay of radio active elements whose abundances depend on the elemental composition as well as the degree of the mixing in the ejecta. In this paper, to simplify the calculation of dust formation, we assume that formation of CO and SiO molecules is complete, that is, no carbon–bearing grain condenses in the region of C/O < 1 and no Si–bearing grain except for the oxide grains condenses in the

region of Si/O < 1. The effect of incomplete formation of CO molecules has been extensively investigated by Clayton, Liu, & Dalgarno (1999) and Clayton, Deneault, & Meyer (2001) and they have shown that carbon grain can condense even in the region of C/O < 1. Also the formation efficiency of SiO molecules is expected to affect the abundance and the size of Si– and/or Mg–bearing grains. The effect of the formation efficiency of CO and SiO molecules on the dust formation in the ejecta is discussed in Appendix B.

The grain species, the chemical reactions at the condensations and the basic data necessary for dust formation calculations are tabulated in Table 2. The Gibbs free energy for formation of a condensate from the reactants is approximated by a formula $\Delta G_j^0/kT = -A/T + B$ and the numerical values of A and B are evaluated by the least squares' fitting of the thermodynamic data (Chase et al. 1985). It should be recognized here that what kind of grains species really condenses in the gas with a given elemental composition is determined by the competitive process of formation of each grain species, because formation of a grain species depletes the gaseous atoms and molecules available for the condensation of other grains. So in the calculations, formation of all possible condensates tabulated in Table 2 is taken into account simultaneously.

4. The results of calculations and discussions

In this section, the results of calculations of dust formation in the ejecta of ordinary CCSNe and PISNe are presented and discussed. The behaviors of nucleation and growth of dust grains are depicted in section 4.1. The detailed results of the condensation times, the average radii, and the size distribution functions of each grain species formed in the unmixed and mixed ejecta of CCSNe and PISNe are presented and discussed in sections 4.2 and 4.3, respectively. The dependence of the total mass of newly formed grains and that of the mass yield of each grain species on the progenitor mass are given in sections 4.4 and 4.5, respectively. The effects of the explosion energy as well as the amount of ^{56}Ni in the unmixed ejecta on dust formation are investigated in Appendix A, and the effect of the formation efficiency of CO and SiO molecules is discussed in Appendix B.

4.1. The behavior of nucleation and grain growth

Figure 4 depicts the behaviors of nucleation and grain growth as a function of time after the explosion at a location of $M_r = 3.5\ M_\odot$ in the O–Mg–Si layer with the elemental abundances relative to oxygen Si/O $= 2.97 \times 10^{-2}$, Mg/O $= 8.25 \times 10^{-2}$, and Al/O $=$

9.38×10^{-4}; Fig. 4a for the behaviors of nucleation rate $J_j(t)$ and the depletion of the key species Y_{1j}, and Fig. 4b for the number density $n_{\mathrm{gr},j}$ and the average radius $r_{\mathrm{gr},j}$. At this location, the expected condensates are Al_2O_3, Si– and/or Mg–bearing grains. The key species is Al for Al_2O_3 and Mg or SiO for Mg– and/or Si–bearing grains depending on what kind of grain species really condenses.

As the gas cools down with time, it can be clearly shown from Figs. 4a and 4b that the nucleation rate rapidly increases with increasing the supersaturation ratio, and then decreases with the depletion of the key species due to grain growth, thus the nucleation rate has a maximum at a time. This is a typical behavior of nucleation and grain growth in a cooling gas. The time at which the nucleation rate reaches to the maximum is defined as the condensation time. At this location, Al_2O_3 grain condenses first at day 400, and then Mg_2SiO_4 condenses consuming the key species SiO at day 421, and finally the remaining Mg atoms are locked into MgO grains at day 439. Also it should be noted that each grain grows to the final radius in the very short time interval; less than 20 days after the condensation time.

Furthermore, we can see from Figs. 4a and 4b that the smaller abundance of the key species leads to the larger number density of condensation nuclei with broad peak of the nucleation rate and results in the small average radius. Thus, the abundance of the key species is very sensitive to the number density and average radius of newly formed grains, which is well reflected to the size distribution function of grains given in Figure 5; Fig. 5a at $M_r = 3.5\ M_\odot$ and Fig. 5b at $M_r = 4.0\ M_\odot$ where the abundances of Si, Mg and Al are more than one order of magnitude smaller than at $M_r = 3.5\ M_\odot$; $Si/O = 1.50 \times 10^{-4}$, $Mg/O = 6.40 \times 10^{-3}$, and $Al/O = 3.95 \times 10^{-5}$. At $M_r = 4.0\ M_\odot$, the smaller abundance of the key species SiO for formation of Mg_2SiO_4 grains results in the larger number of condensation nuclei with very broad peak of the nucleation rate corresponding to the wide-spreaded size distribution, which is true for formation of Al_2O_3 grains. On the other hand, the size distribution function of MgO grains at $M_r = 4.0\ M_\odot$ is almost the same as that at $M_r = 3.5\ M_\odot$, because the abundance of Mg being the key species for formation of MgO and remaining after the formation of Mg_2SiO_4 is only factor 4 smaller at $M_r = 4\ M_\odot$ than at $M_r = 3.5\ M_\odot$. Note that the size distribution function of a grain species formed at a location is approximately log–normal so far as the average size is larger than $\sim 0.01\ \mu$m.

4.2. The dust formation in unmixed ejecta of CCSNe and PISNe

In the unmixed ejecta of supernovae, a variety of grain species condense in each layer corresponding to the difference in the elemental composition. Fig. 6a and Fig. 6b show the

condensation times of dust grains formed in the unmixed ejecta of C20 and P170, respectively. At first carbon grains condense in the He–layer, which is followed by the condensation of Al_2O_3 and Mg–silicates (Mg_2SiO_4 and $MgSiO_3$) in the oxygen–rich layer, MgO in the O–Mg–Si layer, SiO_2 in O–Si–Mg layer, Si and FeS inside Si–S–Fe layer, and Fe in the innermost Fe–Si–S layer in this sequence. Note that in the O–Si–Mg layer SiO_2 grains condense from SiO molecules left over after the formation of Mg–silicate grains, otherwise MgO grains condense from Mg atoms remaining in the O–Mg–Si layer. The major grain species are Mg_2SiO_4 and MgO in the O–Mg–Si layer, otherwise $MgSiO_3$ and SiO_2 in the O–Si–Mg layer. In the ejecta of C20, Si grains condense in the innermost region of the He–layer because a significant amount of Si atoms are present around the interface between He–layer and oxygen–rich layer (see Fig. 1a), but no SiC grain condenses in this region. Anyway, in the unmixed ejecta of C20 and P170, the grain species condensed in the ejecta are the same. Also metallic Cr and Ni grains do not condense significantly in the Fe–Si–S layer of the both ejecta because of the low number density as well as the high energy barrier for nucleation.

The condensation time generally depends not only on the temporal evolution of gas temperature but also on the concentration of the key species at the formation site. On the other hand, given the time evolution of gas temperature, the condensation temperature defined as the gas temperature at the condensation time depends only on the concentration of the key species; the condensation temperature decreases with decreasing the concentrations. In the unmixed ejecta of CCSNe and PISNe, the condensation temperature does not heavily depend on the progenitor mass; ~ 1900 K for carbon, 1600–1700 K for Al_2O_3, 1400–1500 K for Mg–silicates, 1350–1450 K for MgO, 1300–1400 K for SiO_2, 1100–1200 K for Si, 1000–1100 K for FeS and 800–850 K for Fe. The reason is as follows; as described in section 2, the concentration of the key species is a few times large in the ejecta of PISNe compared with CCSNe, and the elemental composition in each layer and the gas density at a time are not so significantly different between CCSNe and PISNe. On the other hand, the gas temperature in the ejecta of PISNe is higher than that of CCSNe. Thus, as can be seen from Figs. 6a and 6b, the condensation time of each grain species in the ejecta of PISNe is about 150 days delayed in comparison with that of CCSNe. Anyway, dust grains condense in the ejecta of ordinary CCSNe around day 300 to 600 after the explosion, and around day 500 to 800 in the ejecta of PISNe, which is almost independent of the progenitor mass.

Figures 7a and 7b show the average radius of each grain species in the ejecta of C20 and P170, respectively. The average radius of each grain species well reflects the concentration of the key species at the condensation time, and heavily depends on the elemental composition and the gas density at the formation site in the ejecta. In the ejecta of C20, the average radii of Fe and Si condensed in the innermost region are relatively large; about 0.2 μm for Fe and 0.4 μm for Si. The range of the average radius spans about one order of magnitude for

carbon, Al_2O_3, SiO_2 and FeS whose maximum radii are 0.4 μm, 0.004 μm, 0.1 μm and 0.06 μm, respectively. The range spans more than two orders of magnitude for MgO, Mg_2SiO_4, and $MgSiO_3$ with the maximum radii 0.2 μm, 0.1 μm and 0.5 μm, respectively. In the ejecta of P170, the average radius of each grain species is a little smaller than that in the ejecta of C20, but the difference is not significant except for Fe, FeS and Si condensed in the Fe–Si–S layer where the gas density is substantially lower than that in the ejecta of C20 (see Fig. 2). The average radii of dust grains formed in the unmixed ejecta are limited to less than 1 μm.

The size distrubution functions of newly formed grains in the ejecta of C20 and P170 are given in Figs. 8a and 8b, respectively. As is shown in § 4.1, the size distribution function at a location is approximately log–nomal for a grain species with the average radius larger than $\sim$ 0.01 μm. However, the size distribution function of a grain species summed up over the formation region does not keep the original shape at the formation site, reflecting the difference of the elemental composition and the gas density in the formation region. Generally, for a grain species whose formation region is wide–spreaded in the ejecta and whose average radius spans more than one order of magnitude, the size distribution function completely deviates from the original log–normal shape, which is true for MgO, Mg_2SiO_4, $MgSiO_3$ and FeS grains. Although the average size of carbon grains ranges from 0.01 to 0.4 μm, the size distribution function looks like log–normal because the large grains formed in the innermost region of He–layer do not contribute to the size distribution function due to the small number compared with the small grains condensed in the outer He–layer. The size distribution functions of SiO_2 and Fe in the ejecta are approximately log–normal. Si grain shows a bimordial distribution function with large grains condensed inside the Si–S–Fe layer and smaller ones condensed around the interface between the He–layer and the O–Mg–Si layer. In the ejecta of P170, the behavior of the summed up size distribution function of each grain species is the same as that in the ejecta of C20. However, in the ejecta of P170, the bimordiality of Si stems from the wide span of the average radius arising from the density variation within the Fe–Si–S layer.

The size distribtion function summed up over all grain species formed within the He–core is drawn by the thick curve in Figure 8. The thick straight lines represent power–law formulae with the index of $\alpha = -3.5$ and $\alpha = -2.5$. As can be seen from Fig. 8, in the both cases, the size distribution summed up over all grain species is well fitted with a power–law formula whose index is -3.5 for the larger size and -2.5 for smaller one, which is different from the conventional MRN size distribution function (Mathis, Rumpl, & Nordsieck 1977) used in the astrophysical literatures. The radius at the crossover point is 0.06 μm for C20 and 0.02 μm for P170. Although in this subsection only one model for CCSNe and PISNe is presented, respectively, the behaviors of dust formation and the average size as well as the size distribution function described above are almost the same for the other models, being

not dependent on the progenitor mass.

4.3.   The dust formation in uniformly mixed ejecta of CCSNe and PISNe

This subsection presents the results of the dust formation calculations in the ejecta with the elemental composition uniformly mixed within the He–core as a extreme case. In the calculations we assume the density structure in the ejecta is not affected by the mixing, since the numerical simulation suggested that the Rayleigh–Taylor instability produces the clumpy structure but the gas density does not so much change on average (Hachisu et al. 1990).

Under the assumption that formation of CO molecules is complete, only oxide grains condense in the uniformly mixed ejecta because the ejecta is oxygen–rich. Figure 9 shows the condensation time of each grain species formed in the ejecta; Fig. 9a for C25 and Fig. 9b for P200. In the both models, Al_2O_3, Mg–silicates (Mg_2SiO_4 and $MgSiO_3$), SiO_2 and Fe_3O_4 grains condense in this order. Being different from the unmixed ejecta, no MgO grain condenses because of $Si > Mg$ in the uniformly mixed ejecta, and all iron atoms are locked into Fe_3O_4 grains. Except for the inner– and outermost region of P200, the condensation temperature of each dust grains is almost the same within the He–core; 1550–1600 K for Al_2O_3, 1450 K for Mg–silicates, 1350 K for SiO_2 and 1300–1350 K for Fe_3O_4.

In the ejecta of C25, the gas temperature decreases faster in the outer region than in the inner region of $M_r \leq 6.8~M_\odot$ where the gas temperature at a time t is almost the same. Thus, well reflecting the temperature structure in the ejecta, in the ejecta of C25, Al_2O_3 grains start to condense at day 330 in the outer edge of He–core after the explosion, Mg–silicate grains at day 350, SiO_2 grains at day 364, and Fe_3O_4 at day 370. In the region of $M_r \leq 6.8~M_\odot$, each grain species condenses at almost the same time; Al_2O_3 around day 385, Mg–silicates around day 400, SiO_2 around day 415 and Fe_3O_4 around day 420. Being different from the formation of dust grains in the unmixed ejecta, all dust grains condense within 100 days after the onset of dust formation. On the other hand, in the ejecta of P200, the condensation time of each grain species increases with decreasing the mass coordinate because the gas density gradually decreases with decreasing M_r; Al_2O_3 grains from day 450 up to day 560, Mg–silicate grains from day 450 up to 570, SiO_2 grains from day 465 up to day 583, and Fe_3O_4 grains from day 470 to day 590. In the ejecta of P200, the condensation times of dust grains are about 150 days later than those in the ejecta of C25 since the gas temperature at a given time is higher than that of C25.

As are shown in Fig. 10a for C25 and Fig. 10b for P200, the range of average radius of

each grain species spans less than one order of magnitude throughout the He–core. Given the same elemental composition within the He–core, the average radius depends on not only the density structure of gas but also the time evolution of gas temperature; in the outer region of the He–core, the gas density is lower than that in the inner region, but the gas temperature decreases faster in the outer region, which compensates the decrease of gas density at the condensation time. In the inner region of P200, the gas temperature is almost the same being independent of M_r and the variation of the gas density is less than one order of magnitude. In the mixed ejecta of C25, the average radii of SiO_2 and Mg–silicates are a few hundredth μm with the maximum 0.1 μm for SiO_2, 0.05 μm for Mg_2SiO_4 and 0.07 μm for $MgSiO_3$. The average radii of Fe_3O_4 and Al_2O_3 are small; several tens Å for Fe_3O_4 and a several AA for Al_2O_3 which are consistent with the results by Todini and Ferrara (2001). Despite that the gas temperature in the mixed ejecta of P200 is higher than that of C25, the average radius of each grain species formed in the region of $M_r > 40\ M_\odot$ is almost the same as that in the ejecta of C25, because abundance of the key species of dust grains is a few times larger in P200 than in C25. The low density in the region of $M_r < 40\ M_\odot$ of P200 (see Fig. 2b) results in the smaller average radius for each grain species.

Figure 11 shows the size distribution function of each dust grains formed in the mixed ejecta; Fig. 11a for C25 and Fig. 11b for P200. Except for Al_2O_3 grains with very small average radius, in the both models, the size distribution functions of Mg_2SiO_4, $MgSiO_3$, SiO_2 and Fe_3O_4 grains approximately tend to be log–normal because of the narrow size range of each grain species. The size distribution function summed up over all grain species is also fitted with a power–law formula, whose index is -3.5 for radius larger than 0.004 μm in P200 and -2.5 for radius smaller than 0.02 μm in C25. The deviation from the power–law formula is distinctive for the larger size in the model of C25, because only SiO_2 grain with the log–normal distribution function contributes to the larger size. However, this is an untypical case for the behavior of the summed up size distribution function. Here it should be addressed that, irrespective of the progenitor mass, the size distribution function summed up over all grain species newly formed in the ejecta with and without mixing is approximated by power–law distribution whose index is -3.5 for larger radius and -2.5 for smaller one, although the radius at the crossover point depends on the model of supernovae with the range from 0.004 to 0.1 μm.

4.4.   The amount of freshly formed dust grains

Figure 12 shows the total mass of dust grains produced in the ejecta versus the progenitor mass; Fig. 12a for CCSNe and Fig. 12b for PISNe, where open triangle denotes the results

of calculations for the unmixed ejecta and open square for the mixed ejecta. In Fig. 12a, for a reference, the results of calculations in the unmixed ejecta of HNe are also plotted by cross for H25A and H30A, and open circle for H25B and H30B. The straight lines in Fig. 12a and in Fig. 12b are the linear least squares' fits to the calculated mass for ordinary CCSNe and linearly connect the two data points for PISNe, respectively; solid line for the unmixed ejecta and dashed line for the mixed ejecta.

The total mass of newly formed grains increases with increasing the progenitor mass in the both unmixed and mixed ejecta of CCSNe and PISNe. In the unmixed ejecta of ordinary CCSNe, the total dust mass is 0.57 $M_\odot$ for C20 and 1.32 $M_\odot$ for C30. It is generally expected that the amount of dust grains is more in the mixed ejecta than in the unmixed ejecta because much more oxygen atoms are locked into dust grains in the mixed ejecta. However, in the mixed ejecta of C13, the total mass of dust grains is 0.22 $M_\odot$ and is a little smaller than the dust mass 0.23 $M_\odot$ in the unmixed ejecta. The reason is that in the mixed ejecta of C13, formation of CO molecules consuming the oxygen atoms available for oxide grains limits the amount of oxide grains; in this case, a small amount of Si and FeS grains condense instead of SiO_2 and Fe_3O_4 grains. Also in the model of C25, the dust mass in the mixed ejecta is not so much different compared with that in the unmixed ejecta, because in the model of C25 the He–layer massive compared with other CCSNe somehow depresses the increase in the amount of mass available for formation of oxide grains within the oxygen–rich layer.

In the unmixed ejecta of hypernovae with the same $M(^{56}Ni) = 0.07\ M_\odot$ as CCSNe, H25A and H30A produce almost the same dust mass as C25 and C30, respectively. On the other hand, with a deep mass cut corresponding to $M(^{56}Ni) = 0.7\ M_\odot$, H25B and H30B produce the dust grains about 0.7 $M_\odot$ larger than C25 and C30, respectively. In the ejecta of the CCSNe except for the model of H25 and H30, the ratio of dust mass to the progenitor mass is 0.02–0.05, which increases with increasing the progenitor mass. Although the total mass of newly formed grains depends on the detailed elemental composition in the ejecta as well as the position of mass cut, in general, the total mass produced in the mixed ejecta becomes larger than that in the unmixed ejecta with increasing M_{pr}.

PISNe, for which the progenitor is very massive and is completely disrupted, produce much more dust grains than CCSNe. For the model P200, the total mass of newly formed grains is $\sim 40\ M_\odot$ in the unmixed ejecta and $\sim 60\ M_\odot$ in the mixed ejecta. The mass ratio of newly formed grains to the progenitor mass for PISNe reaches to 0.15–0.3 at least, and the ratio increases with increasing the progenitor mass. Therefore, in the early universe, much more dust grains could be produced and be injected into interstellar space if the very massive stars populate the first generation stars.

4.5. The mass yield of each grain species

Figures 13 and 14 present the mass yield of each grain species versus the progenitor mass M_{pr} in the unmixed ejecta and the mixed ejecta, respectively; Figs. 13a and 14a for CCSNe, and Figs. 13b and 14b for PISNe. In the figures, the smooth curves are the least squares' spline fits to the calculated values for CCSNe and are the straight lines connecting the two calculated values in linear scale for PISNe. Thus for PISNe, the mass yield for a given progenitor mass should be taken as a nominal value.

In the unmixed ejecta of CCSNe (Fig. 13a), with increasing M_{pr}, the mass yield of carbon grains, apart from the small fluctuation, somehow increases up to around $M_{pr} = 25$ $M_\odot$, and then decreases, while the yields of other grain species except for Fe grain increase. The grain species contributing to the total dust mass heavily depend on the progenitor mass for $M_{pr} \leq 28$ $M_\odot$; in the ejecta with $M_{pr} < 15$ $M_\odot$, the major grain species in mass are carbon, Fe and Si grains with the average radius ≥ 0.1 μm. With increasing M_{pr}, the masses of the oxygen–rich layer as well as of the Si–S–Fe layer increase. Therefore, the yields of Si and Mg_2SiO_4 increase, and also the mass of FeS increases together with decreasing the mass of Fe. Around $M_{pr} = 20$ $M_\odot$, Mg_2SiO_4, Si and FeS grains tend to dominate the mass abundance. Around $M_{pr} = 25$ $M_\odot$, the major grain species are Mg_2SiO_4, Si and C grains. The mass abundances of FeS, SiO_2 and MgO grains are larger than that of carbon grain for $M_{pr} \geq 28$ $M_\odot$, and Mg_2SiO_4 and Si are the major grain species followed by MgO, SiO_2 and FeS grains. Although the masses of Al_2O_3 and $MgSiO_3$ grains increase with M_{pr}, their mass fractions are limited to less than 10^{-2}.

The masses of Mg_2SiO_4 and MgO grains per supernova are almost constant in the unmixed ejecta of PISNe, being almost independent of the progenitor mass (see Fig. 13b); $M(Mg_2SiO_4) \simeq 6$ $M_\odot$ and slightly decreases with increasing M_{pr}, and $M(MgO) = 1.4$ $M_\odot$. When the progenitor mass is smaller than 160 $M_\odot$, Mg_2SiO_4, Si, and SiO_2 grains are the major grain species contributing to the total mass. In contrast to the unmixed ejecta of CCSNe, the mass fraction of carbon grain is to be less than 5×10^{-2} although the mass of carbon grains increases with increasing M_{pr}. It should be noted here that for $M_{pr} > 160$ $M_\odot$, the most abundant grain species in the unmixed ejecta of PISNe is Si grain followed by SiO_2 grains, because the masses of the Si–S–Fe layer and the O–Si–Mg layer increase with increasing M_{pr}. Also the mass fractions of iron–bearing grains (Fe and FeS) produced within the Si–S–Fe layer are larger than that of Mg_2SiO_4 grains for $M_{pr} > 220$ $M_\odot$.

In the mixed ejecta of CCSNe (see Fig. 14a), SiO_2 and Mg_2SiO_4 grains mainly contribute to the total dust mass for $M_{pr} \leq 15$ $M_\odot$. The mass of Fe_3O_4 for $M_{pr} \geq 20$ $M_\odot$ is ~ 0.09 $M_\odot$, being almost independent of the progenitor mass. With increasing M_{pr}, the mass of Mg_2SiO_4 increases and reaches to the same as that of SiO_2 at $M_{pr} = 30$ $M_\odot$. The dust mass

of massive CCSNe with $M_{\mathrm{pr}} \geq 25\ M_\odot$ is dominated by SiO_2 and Mg_2SiO_4 grains. Although the yield of Al_2O_3 increases with increasing M_{pr} and tends to be the same mass as Fe_3O_4, the mass fraction of Fe_3O_4 is limited to less than 0.1 for $M_{\mathrm{pr}} \geq 20\ M_\odot$ and that of Al_2O_3 is limited to less than 0.02 at most. In the mixed ejecta of PISNe (see Fig. 14b), SiO_2 is the most abundant grain, regardless of the progenitor mass. As is the same as the mixed ejecta of CCSNe, around the low–mass end of the progenitor mass of PISNe, SiO_2 and Mg_2SiO_4 contribute to the total mass. As the progenitor mass increases, the masses of $MgSiO_3$ and Fe_3O_4 increase and approach to the almost the same mass, while the amount of Mg_2SiO_4 decreases. The total mass of dust grains is dominated by SiO_2, $MgSiO_3$ and Fe_3O_4 whose mass fractions are ~ 0.7, 0.15 and 0.15, respectively.

5. Summary

We investigated the dust formation in the ejecta of population III core collapse and pair–instability supernovae, employing the hydrodynamical models and the results of nucleosynthesis calculations by Umeda and Nomoto (2002). The time evolution of gas temperature in the ejecta is calculated by solving the radiative transfer equation together with the energy equation taking into account of the energy deposition from radio active elements. Two extreme cases are considered for the elemental composition within the He–core; the unmixed case and the uniformly mixed case. In order to clarify what kind of grain species condenses in the ejecta, formation of all possible condensates is calculated simultaneously by applying a theory of non–steady state nucleation and grain growth under the assumption of complete formation of CO and SiO molecules. The results of the calculations are summarized as follows;

(1) The species of newly formed dust grains are affected by the elemental composition in the ejecta. In the unmixed ejecta, a variety of grain species condense corresponding to the elemental composition at the formation site; C and Si grains in the He–layer, Al_2O_3, Mg_2SiO_4 and $MgSiO_3$ grains in the oxygen–rich layer (O–Mg–Si and O–Si–Mg layers), MgO grain in the O–Mg–Si layer, SiO_2 grain in the O–Si–Mg layer, Si and FeS grains in the Si–S–Fe layer and Fe grain in the Fe–Si–S layer. On the other hand, only oxide grains such as Al_2O_3, Mg_2SiO_4, $MgSiO_3$, SiO_2 and Fe_3O_4 condense in the mixed ejecta. The main species of newly formed grains do not depend on the progenitor mass.

(2) The average size of newly formed dust grains strongly depends on the concentration of the key species at the condensation time as well as at the formation site. In the unmixed ejecta, the range of average radius of each grain species spans a few orders of magnitude, depending on the grain species and the formation region. On the other hand, in the mixed

ejecta, the average radius of each grain species is almost the same order of magnitude in the entire region within the He–core, reflecting the uniform elemental composition. The average radius of each grain species in both the unmixed and the mixed ejecta does not strongly depend on the progenitor mass and the explosion energy, but is affected by the amount of ^{56}Ni in the ejecta. No dust grain condenses with the average radius larger than 1 μm in the ejecta of population III supernovae considered in this paper.

(3) The size distribution function of a grain species condensed at a location in the ejecta is almost log–normal so far as the average radius is larger than 0.01 μm. The size distribution function summed up within the He–core is log–normal for carbon, Fe and SiO$_2$ grains condensed in the narrow confined region of the unmixed ejecta, otherwise in the mixed ejecta, except for Al$_2$O$_3$ grain, the summed up size distribution function is log–normal. The size distribution function summed up over all grain species is approximated by a power–law formula with the index of -3.5 for the larger radius and -2.5 for the smaller one, which is true for the unmixed and the mixed cases, being almost independent of the progenitor mass; the radius at the crossover point ranges from 0.004 to 0.1 μm, depending on the model of supernovae.

(4) The total mass of newly formed dust grains increases with increasing the progenitor mass and is generally much more in the mixed case than in the unmixed case. The total mass of dust grains is 2–5 % of the progenitor mass for CCSNe with 13 $M_\odot \leq M_{\mathrm{pr}} \leq 40$ $M_\odot$, and 15–30 % of the progenitor mass for PISNe with 140 $M_\odot \leq M_{\mathrm{pr}} \leq 260$ $M_\odot$.[1] Thus, if PISNe populate the early universe, a large amount of dust grains would be injected into the primordial interstellar medium.

(5) The mass yield of each grain species depends on the progenitor mass. C, Fe and Si grains are the major grains species in the unmixed ejecta of CCSNe with $M_{\mathrm{pr}} < 15$ $M_\odot$. With increasing M_{pr}, Si and Mg$_2$SiO$_4$ grains are getting dominant, and Mg$_2$SiO$_4$ grains is the most abundant for $M_{\mathrm{pr}} \geq 24$ $M_\odot$. In the unmixed ejecta of PISNe, the most abundant grain is Mg$_2$SiO$_4$ for $M_{\mathrm{pr}} < 160$ $M_\odot$, otherwise for $M_{\mathrm{pr}} \geq 160$ $M_\odot$ the most abundant grain is Si followed by Mg$_2$SiO$_4$, SiO$_2$, FeS, and Fe grains. In the mixed ejecta of CCSNe, SiO$_2$ and/or Mg$_2$SiO$_4$ grains are the major grain species contributing to the total mass. Being independent of the progenitor mass, in the mixed ejecta of PISNe, SiO$_2$ grain is the most abundant species, which is followed by Mg$_2$SiO$_4$ grains for $M_{\mathrm{pr}} < 160$ $M_\odot$ and by MgSiO$_3$ and Fe$_3$O$_4$ grains for $M_{\mathrm{pr}} \geq 170$ $M_\odot$.

In the calculations, we treat only the formation of homogeneous grains taking into ac-

---

[1]After submitting this paper to ApJ on 28 June 2003, we have received a preprint from Dr. A. Ferrara, who obtained basically similar results for the mass of dust produced per PISN as ours.

count of the chemical reaction at the condensation but do not consider the possibility for the heterogeneous nucleation on the surface of pre–condensed grains. In fact, the heterogeneous grains consisting of metal–carbide cores and a graphite mantle have been observed in the Murchison meteorite (Bernatowicz et al. 1991, 1996). Also we must consider the possibility of the formation of composite grains such as Fe–Ni–Cr alloy to reveal whether the metal elements of Ni, Co and Cr with relatively small abundance are locked into dust grains in the ejecta of supernovae or not. Also as is discussed in Appendix B, it is very important to investigate the effect of the formation efficiency of CO and SiO molecules on the formation of dust grains in order to clarify what kind of dust grains really condenses in the ejecta of supernovae. These subjects are left for the future work.

Anyway, dust grains in the early universe play a critical role on formation and evolution history of stars and galaxies. The investigation of the nature of dust grains in the early universe is essential not only to investigate the evolution and the structure of the early universe but also to deduce the SFR and the IMF during the evolution of the universe from the relevant observations, because how much dust grains absorb stellar light and re–emit it by thermal radiation depends on the chemical composition, the size distribution and the amount of dust grains residing in interstellar space in galaxies and in intergalactic medium. The evolution of dust grains is determined by the balance between the production in the ejecta of supernovae and the destruction by the interstellar shock as well as the reverse shock penetrating into the ejecta. The efficiency of destruction by shock depends on the chemical composition and the size of dust grains. Therefore, the results of the calculations presented in this paper can be used as the basis to investigate the evolution of dust grains in the early universe.

A. The dust formation in the ejecta of hypernovae

The hypernovae with the explosion energy larger than 10^{52} erg are proposed to reproduce the behavior of observed early light curve of SN 1998bw (Iwamoto et al. 1998; Woosley, Eastman, & Schmidt 1999). Also the analysis of the light curve of SN 1998bw (Nakamura et al. 2001) concluded that the mass of ^{56}Ni in the ejecta is 0.4 $M_\odot$, which is larger than a typical value of 0.07 $M_\odot$ in the ejecta of ordinary CCSNe. Furthermore, Umeda and Nomoto (2002) have claimed that the primordial hypernovae well reproduce the observed elemental

composition in the metal–poor stars; [Zn/Fe] increasing with decreasing [Fe/H] for [Fe/H] ≤ -2.5 (Primas et al. 2000). In this Appendix, we shall perform the calculations of dust formation in the ejecta of population III hypernovae to investigate the effect of the explosion energy as well as the amount of ^{56}Ni in the ejecta on the dust formation. We consider two model; one is H30A with $M_{\rm pr} = 30\ M_\odot$, $E_{\rm exp} = 3 \times 10^{52}$ erg and $M(^{56}{\rm Ni}) = 0.07\ M_\odot$, and another is H30B for which $M_{\rm pr}$ and $E_{\rm exp}$ are the same as H30A but $M(^{56}{\rm Ni}) = 0.7\ M_\odot$.

Fig. 15a shows the condensation time of each dust grains in the unmixed ejecta of H30A with the explosion energy 30 times but $M(^{56}{\rm Ni})$ as same as ordinary CCSNe. The grain species formed in the ejecta and their condensation sequence are almost the same as CCSNe and PISNe, except for Fe; the reason is that in this model with the explosion energy 3×10^{52} erg, the innermost Fe–Si–S layer is not ejected because of a shallow mass cut caused by adjusting $M(^{56}{\rm Ni})$ in the ejecta to $0.07\ M_\odot$. The condensation time of each grain species is about 200 days earlier than CCSNe, because the gas temperature quickly decreases due to the high expansion velocity and the low gas density in the ejecta. However, as can be seen from Fig. 15b, the average radius of each dust grains formed in the ejecta is almost the same as that in the ejecta of CCSNe, because the early condensation time compensates the decrease of gas density at the condensation time.

With $M(^{56}{\rm Ni}) = 0.7\ M_\odot$ and the higher gas temperature at a time than H30A, as is shown in Fig. 16a, the condensation time of each grains species in the ejecta of H30B is about 150 days later than that of H30A. Therefore, the average radii of dust grains formed in the ejecta are a factor 4–10 smaller than those of H30A (see Fig. 16b), depending on the concentration of key species at the formation site. In contrast to H30A, iron grain condenses in the innermost Fe–Si–S layer, reflecting the deep mass cut at $M_r = 4.33\ M_\odot$.

From the results of calculations, we can conclude here that the explosion energy as well as the amount of ^{56}Ni in the ejecta strongly affects the formation of dust grains in the ejecta. In the ejecta with a fixed amount of ^{56}Ni, the higher explosion energy results in the early condensation time because the gas temperature quickly decreases due to the low gas density. However, the average radius of dust grain is not heavily affected because the early condensation time compensates the decrease of gas density at the formation site. On the other hand, the mass of ^{56}Ni in the ejecta strongly affects the average radius of dust grains formed in the ejecta with the same explosion energy. With increasing $M(^{56}{\rm Ni})$, the more delayed condensation time decreases the concentration of key species at the site of dust formation, which results in the smaller size of dust grains. Finally it should be pointed out here that the amount of ^{56}Ni in the ejecta also affects the total mass of dust grains formed in the ejecta as is depicted in Fig. 13a; a large amount of ^{56}Ni in the ejecta with a deep mass cut for a fixed progenitor mass result in the large mass in the ejecta as well as the large total

mass of dust grains, and vice versa.

B. The effect of formation efficiency of CO and SiO molecules on dust formation

In the calculations of dust formation, we assumed the complete formation of CO and SiO molecules. The formation of CO and SiO molecules prior to the dust formation was observed in SN 1987A (e.g., Bouchet & Danziger 1993). Furthermore, the recent observations have suggested that formation of CO molecules is a common phenomenon in the ejecta of CCSNe (e.g., Gerardy et al. 2002). Formation of CO and SiO molecules is usually considered to be complete and controls the chemistry in the astrophysical environments of interest to dust formation such as in the circumstellar envelopes of AGB star. However, in the ejecta of supernovae, these molecules are destroyed by the collisions with high energy electrons as well as with ionized inert gaseous atoms produced by the decay of radio active elements, and the abundance of these molecules is determined by the balance between formation and destruction (Liu & Dalgarno 1994, 1996). Thus, in the ejecta of supernovae, for an example, it is expected that free carbon atoms are available for formation of carbon–bearing dust grains even in the ejecta of C/O < 1. This aspect has been extensively pursued by Clayton, Liu, & Dalgarno (1999) and Clayton, Deneault, & Meyer (2001) to investigate the origin of presolar grains identified as SUNOCONs. The abundances of CO and SiO molecules depend on the abundance of free electrons as well as ionized inert gas. Thus, in this Appendix, to simplify the calculations, we investigate the effect of the formation efficiency of CO and SiO molecules on the dust formation, by referring to the formation efficiency of CO and SiO molecules observed in SN 1987A as a template and introducing the parameters f_C and f_{Si} which represent the mass fractions of C and Si atoms not locked into CO and SiO molecules, respectively.

In the ejecta of SN 1987A, the masses of CO and SiO molecules have been evaluated to be 3–6 $\times 10^{-3}$ $M_\odot$ and 0.4–1 $\times 10^{-3}$ $M_\odot$, respectively, during 300 to 600 days after the explosion (Liu & Dalgarno 1994, 1995), which correspond to $f_C \simeq 0.99$ and $f_{Si} \simeq 0.9$ in the oxygen–rich core. The mass fractions $f_C = 0.99$ and $f_{Si} = 0.9$ being fixed, respectively, Figs. 17a and 17b show the mass of newly formed grain species versus f_{Si} and f_C at the location of $M_r = 3.5$ $M_\odot$ in the O–Mg–Si layer of C20. In the calculations, we consider SiO molecule is the key species for formation of Mg–silicate grains. Of course, formation of Al$_2$O$_3$ grain is not affected by the formation efficiency of these molecules. The mass of C and Si grains increases with increasing f. As can be seen from Fig. 17a, except for the formation of carbon grains, formation efficiency of CO molecules does not influence the

formation of other grain species. Also the formation of carbon grains does not affect the total mass of dust grains at this location since O and Mg atoms are much more abundant than C atoms (see Fig. 1a). The average size of carbon grains increases with increasing f_C but is limited to less than 0.04 μm even for $f_C = 1$. On the other hand, the formation efficiency of SiO molecules strongly affects the mass abundance of Si– and/or Mg–bearing grains; with increasing f_{Si}, the decrease of SiO molecules not only results in the formation of Si grains but also increases the mass of MgO grains with the reduction of mass of Mg_2SiO_4 grains, which is prominent for $f_{Si} \geq 0.1$. The average radii of Si and MgO grains increase and reach to ~ 0.1 μm with increaing f_{Si}, otherwise the average radius of Mg_2SiO_4 grain decreases. At this location, formation efficiency of CO and SiO molecule does not affect the total mass of dust grains because the abundance of C atom is two order of magnitude lower than that of O atom. However, if $f_C = 0.99$ in the outer region of O–Mg–Si layer ($4\ M_\odot \leq M_r \leq 5\ M_\odot$ for C20), much more carbon dust grains could condense and the average radius reach to 0.4 μm ~ 1 μm, depending on the abundance of carbon atom at the formation site.

Finally it should be addressed here that we cannot realize the formation of SiC grains with radius comparable to presolar SiC grains identified as SUNOCONs by changing the parameters f_C and f_{Si}. Formation of SiC grains competes with the formation of carbon and silicon grains; carbon atoms available for formation of SiC grains are locked into carbon grains prior to formation of SiC grains, which is true for silicon atoms. This implies that the amount and size are very small even if SiC grains condense. Therefore, as proposed by Deneault, Clayton, & Heger (2003), a special condition and/or chemical passways might have to be considered in order to realize the formation of SiC grains identified as SUNOCONs.

Anyway, the result of calculation shows that the reduction of formation efficiency of CO and SiO moclules leads to the formation of C and Si grains. Furthermore, the formation efficiency of SiO molecules affects the abundance and the size of Si– and/or Mg–bearing grains. However we must keep in mind that in the calculations the stability of C and Si grains is not taken into account; in the environment with a lot of free oxygen atoms, C and Si grains could be easily oxidized if their sizes would be small, though Clayton, Deneault, & Meyer (2001) have claimed that carbon grain is stable against the oxidation in the oxygen–rich environment. Oxidation of Si grains produces SiO_2 grains and/or evaporates SiO molecules available for formation of Mg–silicate grains, and it may be possible that another chemical passway leads to formation of Mg–silicate grains without SiO molecules, which results in the more oxide grains even if the formation efficiency is very low. These aspects should be pursued to clarify how much as well as what kind of oxide grains really forms in the ejecta of supernovae.

REFERENCES

Amari, S., & Zinner, E. 1997, in AIP Conf. Proc. 402, Astrophysical Implications of the Laboratory Study of Presolar Materials, eds. T. J. Bernatowicz & E. Zinner (New York: AIP), 287

Arendt, R. G., Dwek, E., & Moseley, S. H. 1999, ApJ, 521, 234

Arnett, W. D., Bahcall, J. N., Kirshner, R. P., & Woosley, S. E. 1989, AAR&A, 27, 629

Bernatowicz, T. J., Amari, S., Zinner, E., & Lewis, R. S. 1991, ApJ, 373, L73

Bernatowicz, T. J., Cowsik, R., Gibbons, P. C., Lodders, K., Fegley, B., Jr., Amari, S., & Lewis, R. S. 1996, ApJ, 472, 760

Boni, R. E., & Derge, D. 1956, J. Metals, 8, 53

Bouchet, P., & Danziger, I. J. 1993, A&A, 273, 451

Bromm, V., Coppi, P. S., & Larson, R. B. 2002, ApJ, 564, 23

Chase, M. W., Davies, C. A., Downey, J. R., Frurip, D. J., McDonald, R. A., & Syverud, A. N. 1985, JANAF Thermochemical Tables 3d ed. (J. Phys. Chem. Ref. Data, 14, Suppl. 1)

Chigai, T., Yamamoto, T., & Kozasa, T. 1999, ApJ, 510, 999

Christlieb, N., et al. 2002, Nature, 419, 904

Clayton, D. D., Deneault, E. A.-N., & Meyer, B. S. 2001, ApJ, 562, 480

Clayton, D. D., Liu, W., & Dalgarno, A. 1999, Science, 283, 1290

Colgan, S. W. J., Haas, M. R., Erickson, E. F., Lord, S. D., & Hollenbach, D. 1994, ApJ, 427, 874

Deneault, E. A. -N., Clayton, D. D., & Heger, A. 2003, ApJ preprint doi:10.1086/376863

Dotani, T., Hayashida, K., Inoue, H., Itoh, M., & Koyama, K. 1987, Nature, 330, 230

Douvion, T., Lagage, P. O., Cesarsky, C. J., & Dwek, E. 2001, A&A, 373, 281

Douvion, T., Lagage, P. O., & Pantin, E. 2001, A&A, 369, 589

Drake, R. P., et al. 2002, ApJ, 564, 896

Dunne, L., Eales, S., Ivison, R., Morgan, H., & Edumnds, M. 2003, Nature, 424, 285

Dwek, E. 1998, ApJ, 501, 643

Dwek, E., Hauser, M. G., Dinerstein, H. L., Gillett, F. C., & Rice, W. L. 1987, ApJ, 315, 571

Elliott, J. F., & Gleiser, M. 1960, Thermochemistry for Steelmaking, Vol. 1. Addison-Wesley, Reading, MA.

Elliott, J. F., Gleiser, M., & Ramakrishna, V. 1963, Thermochemistry for Steelmaking, Vol. 2. Addison-Wesley, Reading, MA.

Elmhamdi, A., et al. 2003, MNRAS, 338, 939

Fesen, R., & Blair, W. P. 1990, ApJ, 351, L45

Gail, H.-P., Keller, R., & Sedlmayr, E. 1984, A&A, 133, 320

Gerardy, C. L., Fesen, R. A., Nomoto, K., Maeda, K., Hoflich, P., & Wheeler, J. C. 2002, PASJ, 54, 905

Hachisu, I., Matsuda, T., Nomoto, K., & Shigeyama, T. 1990, ApJ, 358, L57

Hasegawa, H., & Kozasa, T. 1988, Prog. Theor. Phys. Suppl., 96, 107

Hauser, M. G., & Dwek, E. 2001, ARA&A, 39, 249

Heger, A., & Woosley, S. E. 2002, ApJ, 567, 532

Hester, J. J., Graham, J. R., Beichman, C. A., & Gautier, T. N., III 1990, ApJ, 357, 539

Hirashita, H., & Ferrara, A. 2002, MNRAS, 337, 921

Hirashita, H., Hunt, L. K., & Ferrara, A. 2002, MNRAS, 330, L19

Itoh, M., Kumagai, S., Shigeyama, T., Nomoto, K., & Nishimura, J. 1987, Nature, 330, 2331

Iwamoto, K., et al. 1998, Nature, 395, 672

Iwamoto, K., et al. 2000, ApJ, 534, 660

Kozasa, T., Dorschner, J., Henning, T., & Stognienko, R. 1996, A&A, 307, 551

Kozasa, T., & Hasegawa, H. 1987, Prog. Theor. Phys., 77, 1402

————. 1988, ICARUS, 73, 180

Kozasa, T., Hasegawa, H., & Nomoto, K. 1989a, ApJ, 344, 325

————. 1989b, ApJ, 346, L81

————. 1991, A&A, 249, 474

Kumagai, S., Shigeyama, T., Nomoto, K., Itoh, M., & Nishimura, J. 1988, A&A, 197, L7

Lagage, P. O., et al. 1996, A&A, 315, L273

Liu, W., & Dalgarno, A. 1994, ApJ, 428, 769

————. 1995, ApJ, 454, 472

————. 1996, ApJ, 471, 480

Loeb, A., & Haiman, Z. 1997, ApJ, 490, 571

Lucy, L. B., Danziger, I. J., Gouiffes, C., & Bouchet, P. 1989, in Structure and Dynamics of Interstellar Medium, IAU Colloq. No 120, eds. G. Tenorio-Tagle, M. Mole, & J. Melnick (Berlin : Springer), 350, 164

Mathis, J. S., Rumpl, W., & Nordsieck, K. H. 1977, ApJ, 217, 425

Meikle, W. P. S., Spyromilio, J., Allen, D. A., Varani, G. -F., & Cumming, R. J. 1993, MNRAS, 261, 535

Mezger, P. G., Tuffs, R. J., Chini, R., Kreysa, E., & Gemünd, H.-P. 1986, A&A, 167, 145

Nakamura, T., Mazzali, P. A., Nomoto, K., & Iwamoto, K. 2001, ApJ, 550, 991

Nakamura, F., & Umemura, M. 2001, ApJ, 548, 19

Nomoto, K., Maeda, K., Mazzali, P. A., Umeda, H., Deng, J., & Iwamoto, K. 2003, in Stellar Collapse, ed. C. L. Fryer (Dordrecht; Kluwer), in press (astro-ph/0308136)

Nomoto, K., Mazzali, P. A., Nakamura, T., et al. 2001, in Supernovae and Gamma Ray Bursts, eds. M. Livio et al. (Cambridge Univ. Press), 144 (astro-ph/0003077)

Overbury, S. H., Bertrand, P. A., & Somorjai, G. A. 1975, Chemical reviews, 75, 547

Pei, Y. C., & Fall, S. M. 1995, ApJ, 454, 69

Pettini, M., King, D. L., Smith, L. J., & Hunstead, R. W. 1997, ApJ, 478, 536

Pettini, M., Smith, L. J., Hunstead, R. W., & King, D. L. 1994, ApJ, 426, 79

Primas, F., et al. 2000, in The First Stars, ed. A. Weiss, T. Abel, & V. Hill (Berlin : Springer), p51

Rhee, S. K. 1970, J. Am. Ceram. Soc., 53, 639

Robie, R. A., & Waldbaum, D. R. 1968, Geological Survey Bull., No. 1259

Schneider, R., Ferrara, A., Salvaterra, R., Omukai, K., & Bromm, V. 2003, Nature, 422, 869

Schneider, R., Ferrara, A., & Salvaterra, R. 2003, submitted to MNRAS (astro-ph/0307087)

Shigeyama, T., & Nomoto, K. 1990, ApJ, 360, 242

Tabak, R. G., Hirth, J. P., Meyrick, G., & Roark, T. P. 1975, ApJ, 196, 457

Todini, P., & Ferrara, A. 2001, MNRAS, 325, 726

Travaglio, C., Gallino, R., Amari, S., Zinner, E., Woosley, S., & Lewis, R. S. 1999, ApJ, 510, 325

Umeda, H., & Nomoto, K. 2002, ApJ, 565, 385

———. 2003a, Nature, 422, 871

———. 2003b, submitted to ApJ (astro-ph/0308029)

Whitelock, P. A., et al. 1989, MNRAS, 240, 7

Wooden, D. H., Rank, D. M., Bregman, J. D., Witteborn, F. C., Tielen, A. G. G. M., Cohen, M., Pinto, P. A., & Axelrod, T. S. 1993, ApJS, 88, 477

Woosley, S. E., Eastman, R. G., & Schmidt, B. P. 1999, ApJ, 516, 788

Woosley, S. E., & Weaver, T. A. 1995, ApJS, 101, 181

Yamamoto, T., Chigai, T., Watanabe, S., & Kozasa, T. 2001, A&A, 380, 373

Zinner, E. 1998, Meteoritics & Planetary Science, 33, 549
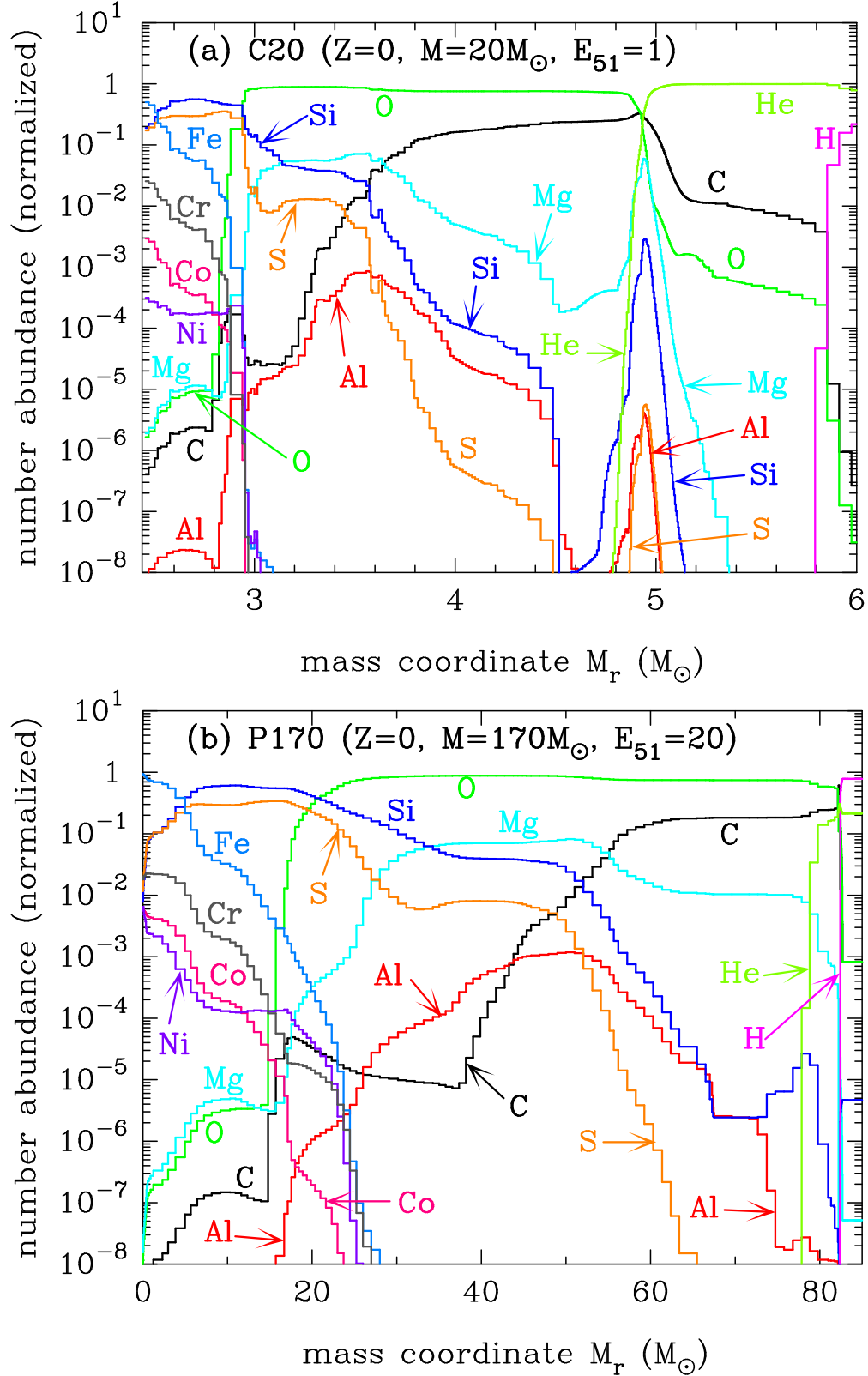
Fig. 1.— The number abundance of elements relevant to dust formation within the unmixed He–core at 600 days after the explosion, taking into account the decay of radio active elements; (a) for C20 and (b) for P170. [*See the electric edition of the Journal for a color version of this figure.*]
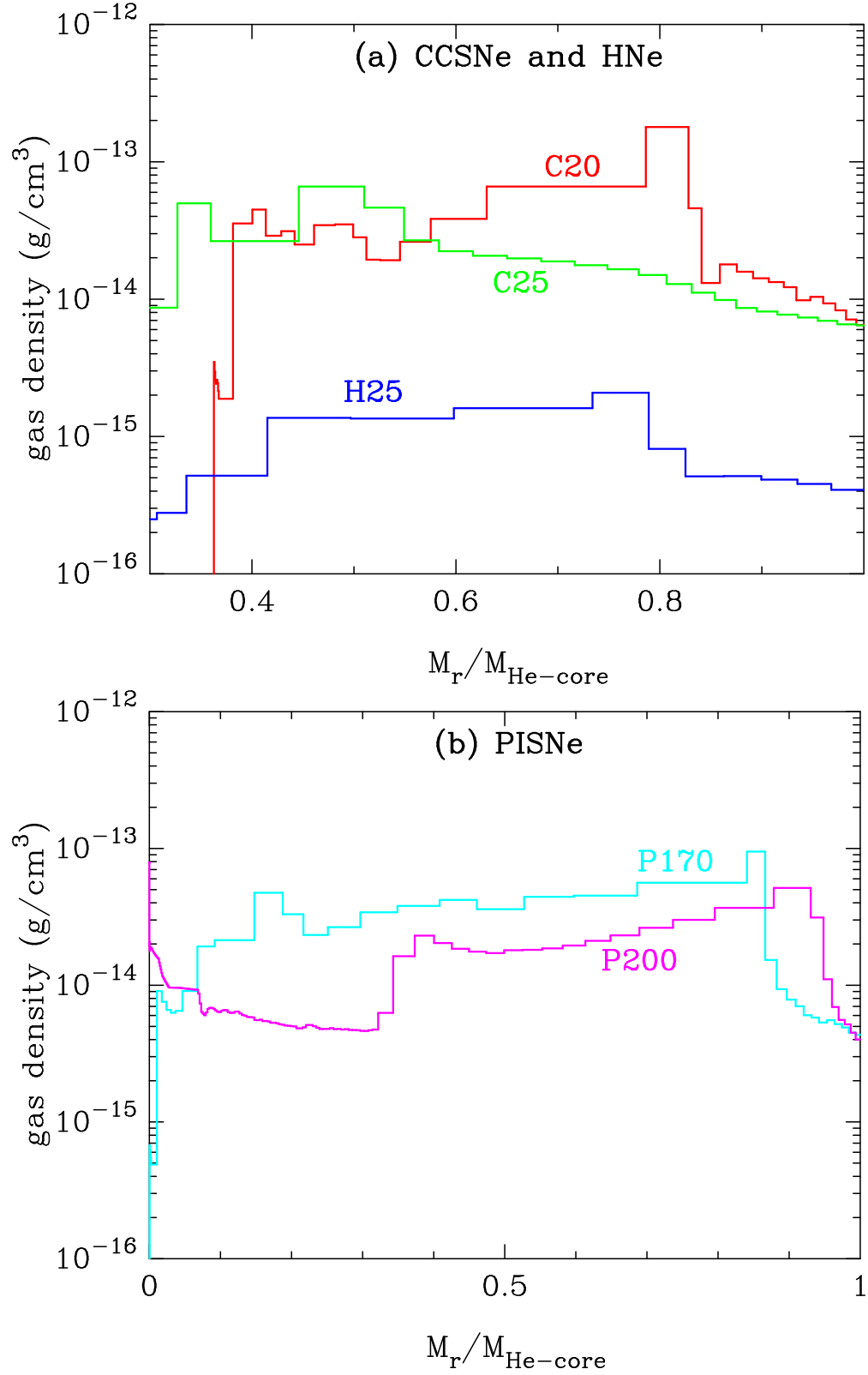
Fig. 2.— The distribution of gas density within the He–core at 600 days after the explosion; (a) for C20, C25 and H25 and (b) for P170 and P200. Note that the mass coordinate is normalized to the He–core mass.
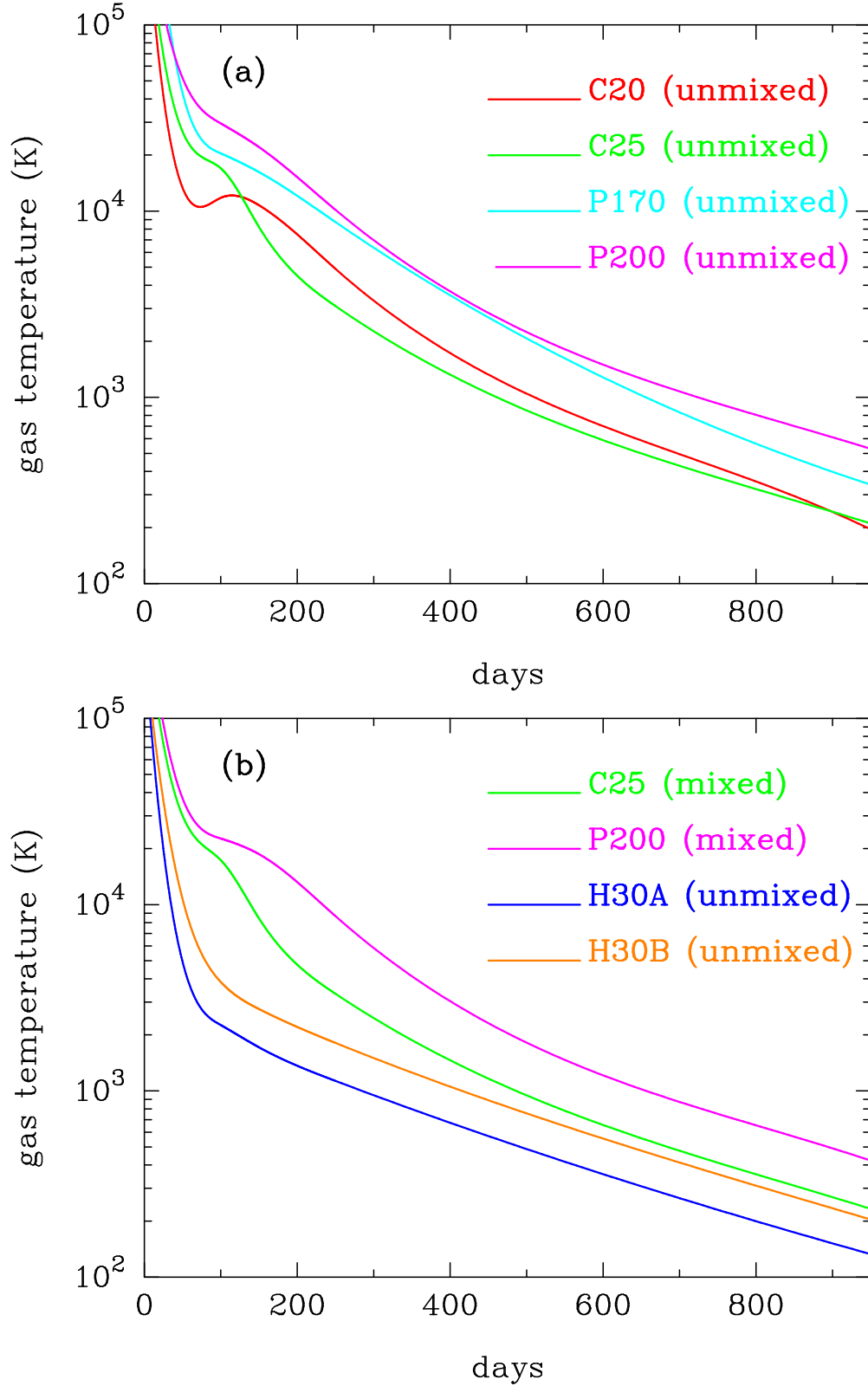
Fig. 3.— The time evolution of gas temperature at a location of the oxygen–rich layer with almost the same elemental composition in the ejecta of CCSNe, PISNe and HNe; (a) at $M_r = 3.7 \ M_\odot$ for C20, at $M_r = 4.6 \ M_\odot$ for C25, at $M_r = 56.5 \ M_\odot$ for P170, and at $M_r = 64.9 \ M_\odot$ for P200 in the unmixed ejecta, (b) at $M_r = 4.6 \ M_\odot$ for C25 and at $M_r = 64.9 \ M_\odot$
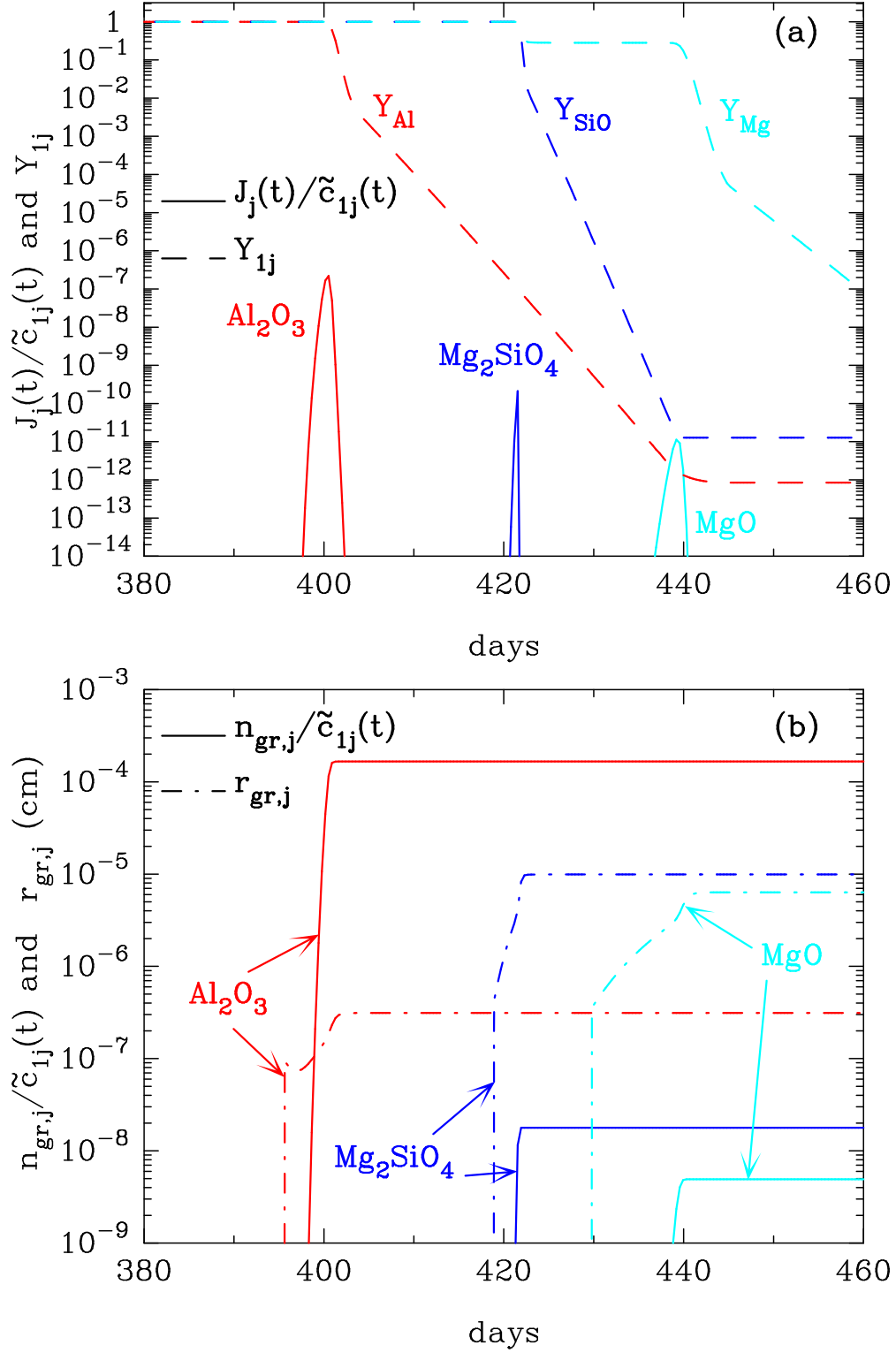
Fig. 4.— The behaviors of nucleation and growth of each grain species condensed at $M_r = 3.5\ M_\odot$ in the O–Mg–Si layer of the unmixed ejecta for C20; (a) the time evolution of the nucleation rate $J_j(t)$ normalized to $\tilde{c}_{1j}(t)$ (solid line) and the depletion of key species Y_{1j} (dashed line), (b) the time evolution of the number density $n_{gr,j}$ normalized to $\tilde{c}_{1j}(t)$ (solid line) and the average grain radius $r_{gr,j}$ (dot–dashed line). The number abundances of dust forming elements relative to oxygen at this location are Si/O $= 2.97 \times 10^{-2}$, Mg/O
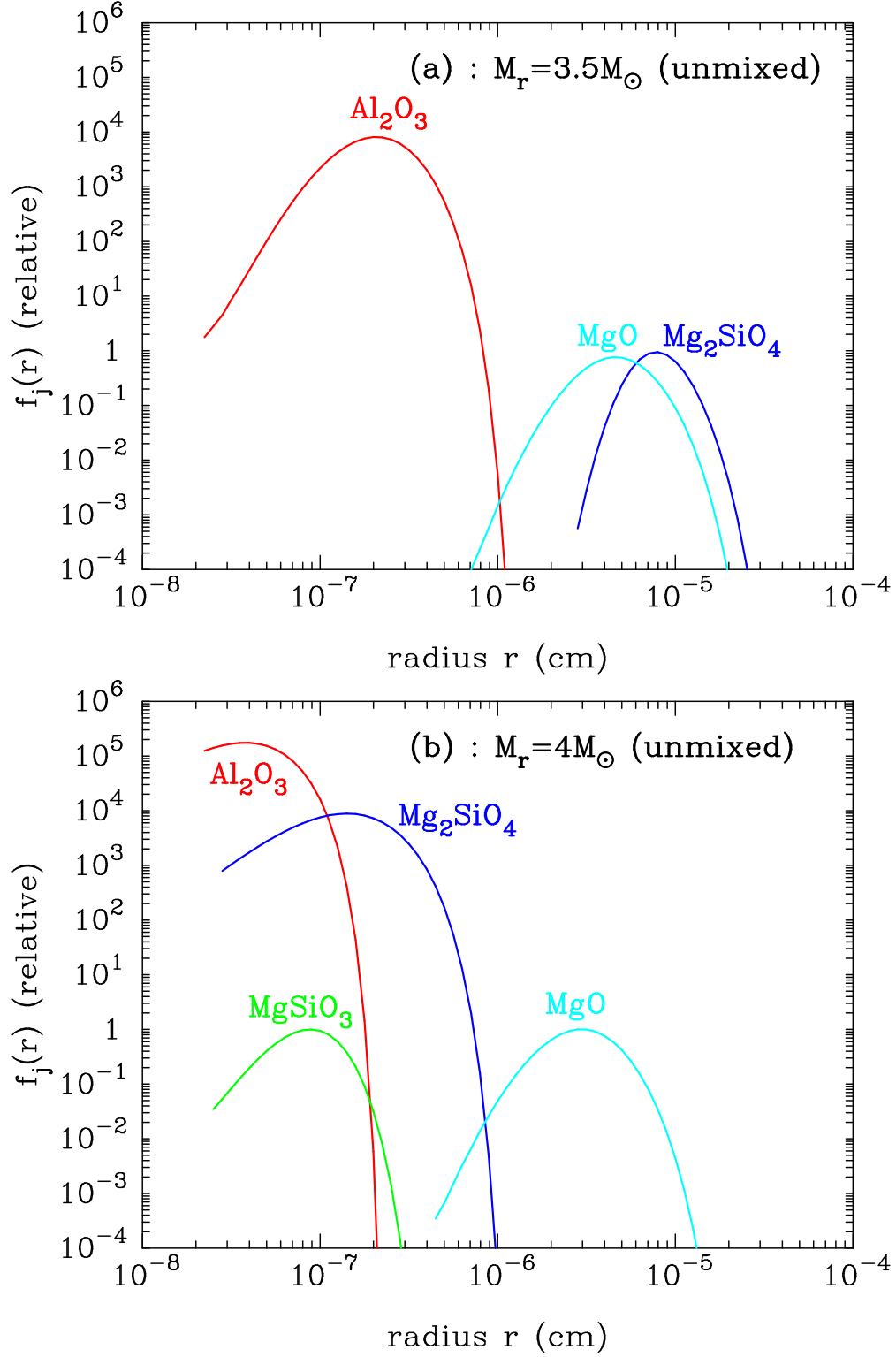
Fig. 5.— The size distribution function of each grain species formed at a location in the O–Mg–Si layer of the unmixed ejecta for C20; (a) at $M_r = 3.5\ M_\odot$ and (b) at $M_r = 4\ M_\odot$ with Si/O $= 1.50 \times 10^{-4}$, Mg/O $= 6.40 \times 10^{-3}$, and Al/O $= 3.95 \times 10^{-5}$.
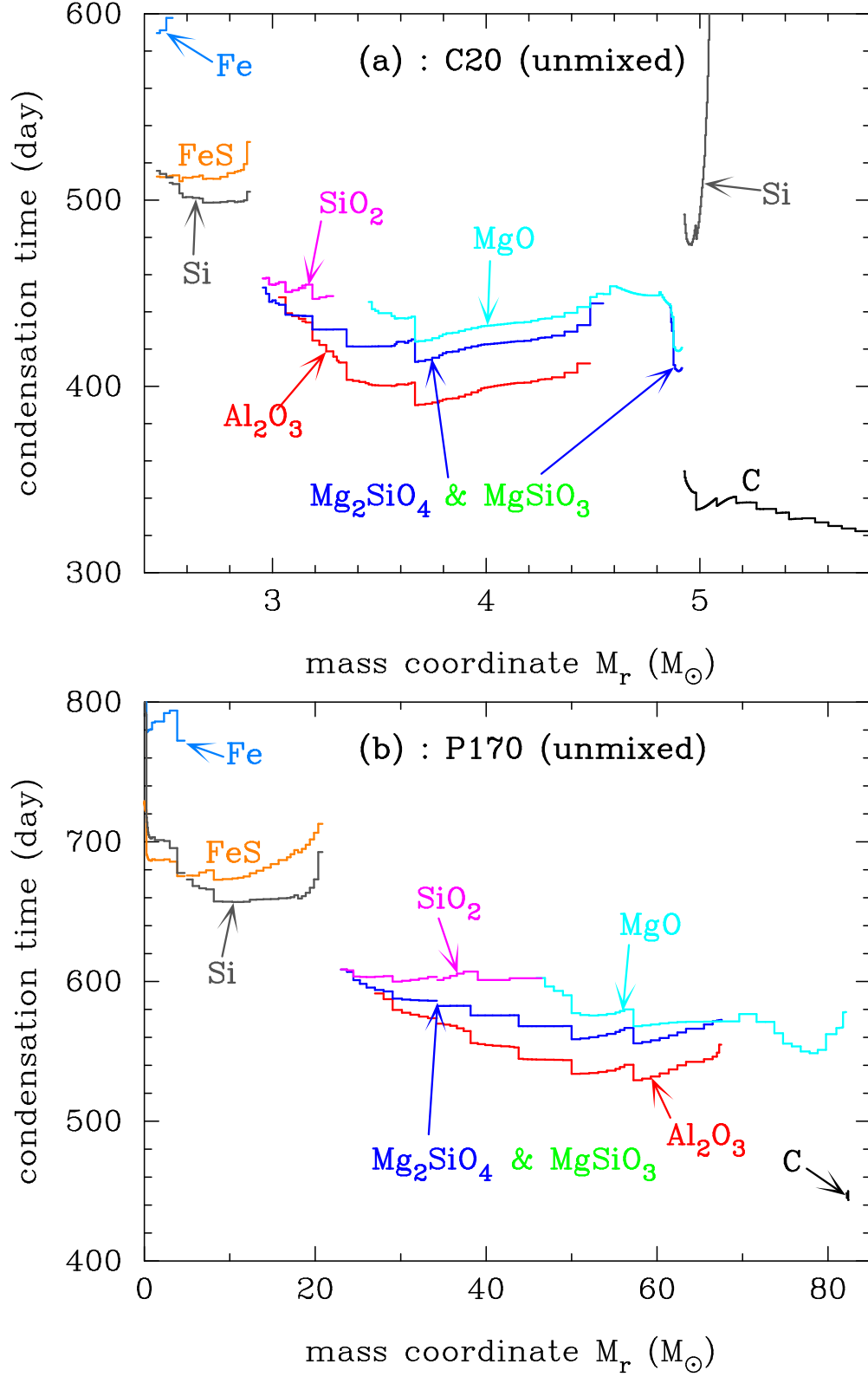
Fig. 6.— The condensation times of dust grains formed in the unmixed ejecta; (a) for C20 and (b) for P170. [*See the electric edition of the Journal for a color version of this figure.*]
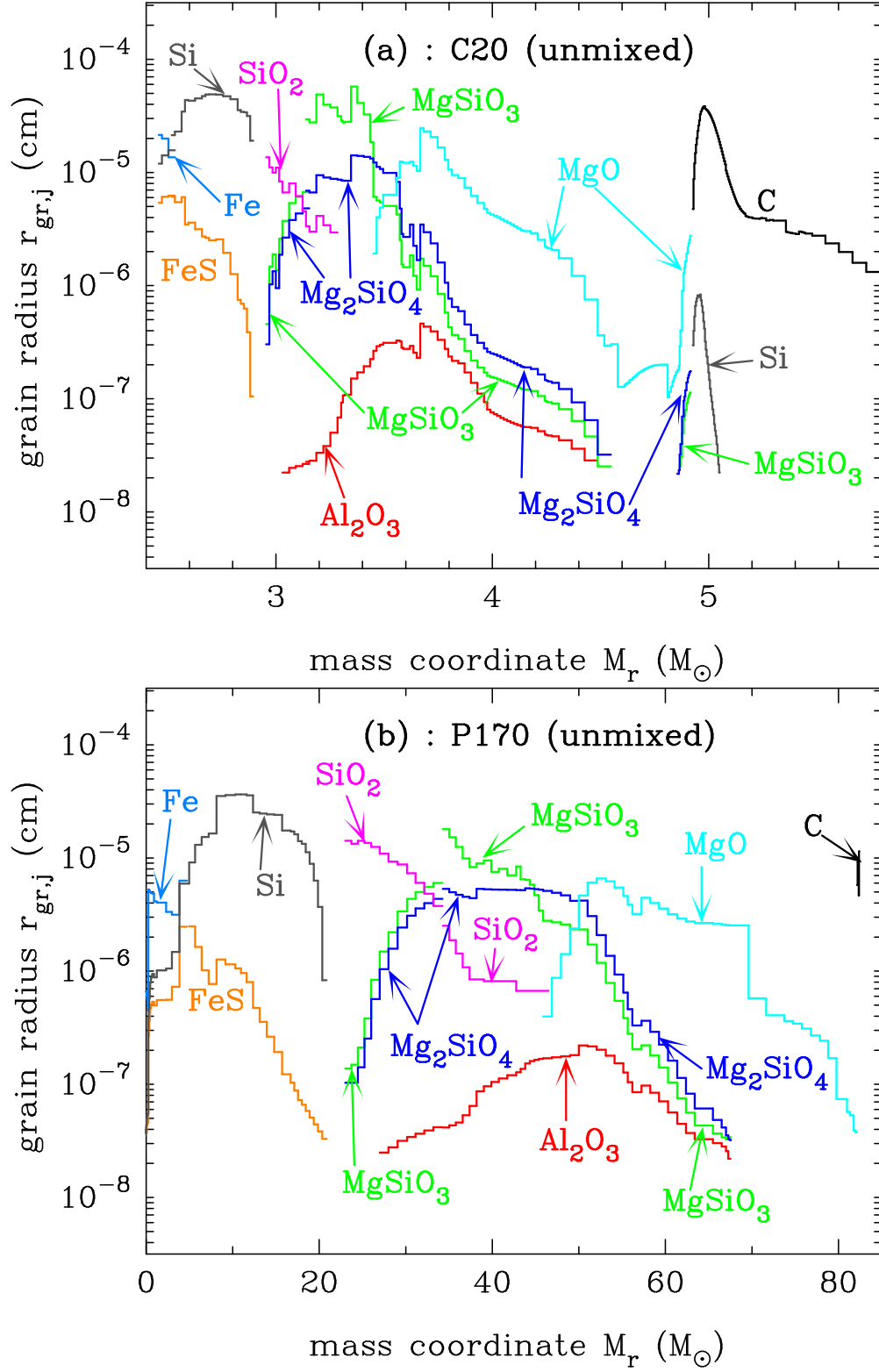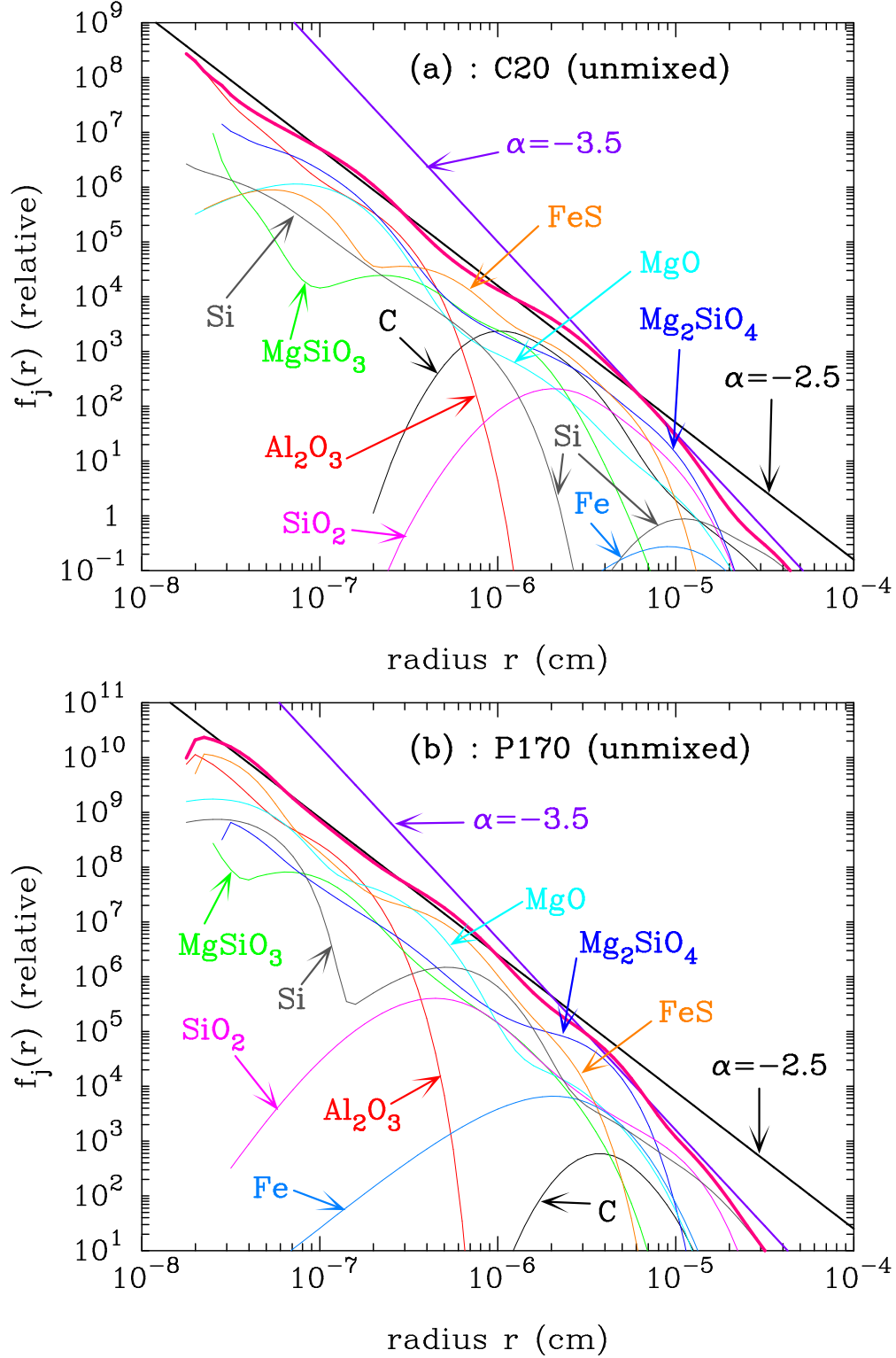
Fig. 7.— The average radii of dust grains formed in the unmixed ejecta; (a) for C20 and (b) for P170. [*See the electric edition of the Journal for a color version of this figure.*]

Fig. 8.— The size distribution function of each grain species summed up over the formation region in the unmixed ejecta. The thick curve represents the size distribution function summed up over all grain species and the straight lines indicate power–law formulae with the index of $\alpha = -2.5$ and $\alpha = -3.5$; (a) for C20 and (b) for P170. [*See the electric edition of the Journal for a color version of this figure.*]
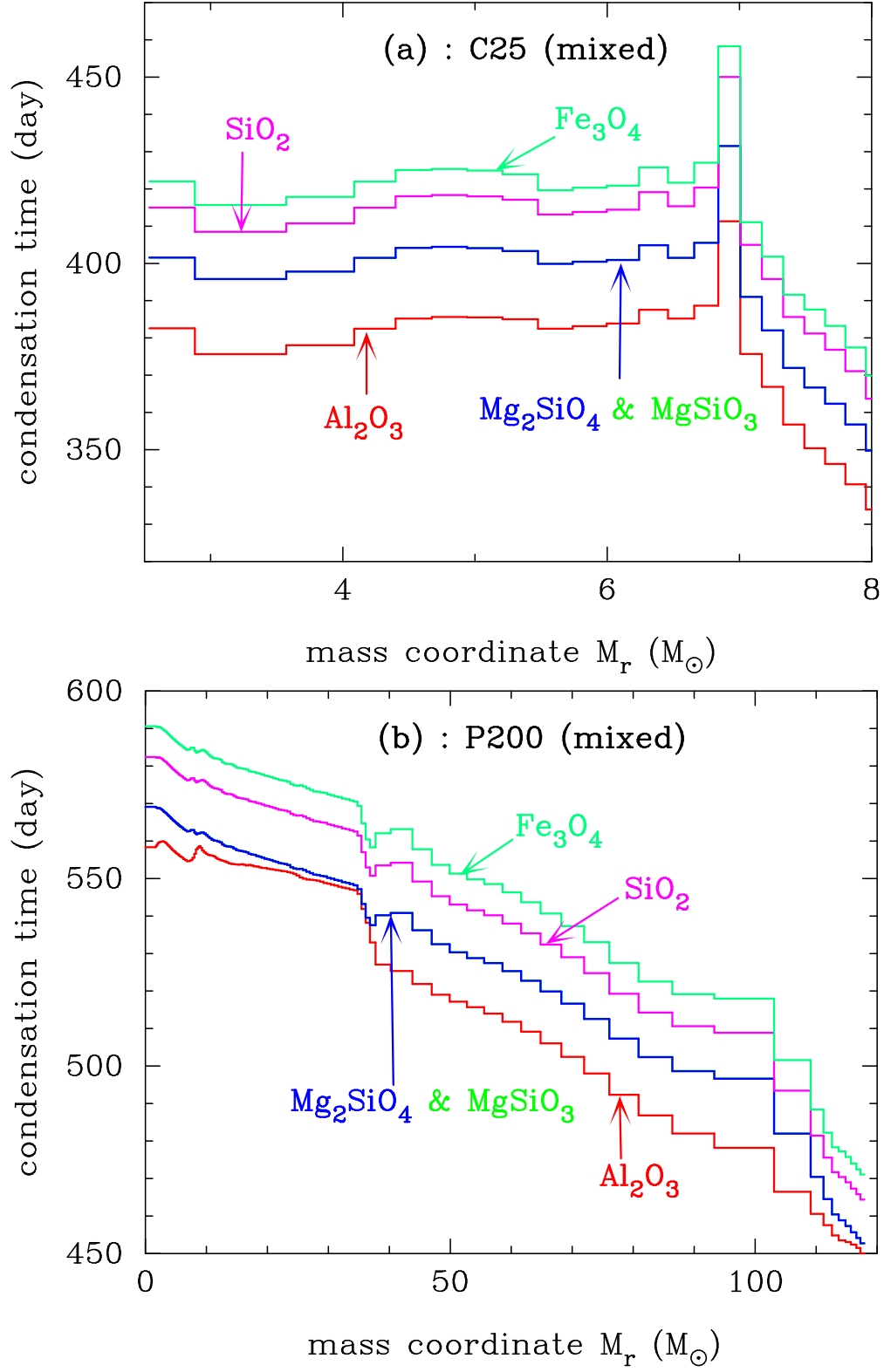
Fig. 9.— The condensation times of dust grains formed in the mixed ejecta; (a) for C25 and (b) for P200. [*See the electric edition of the Journal for a color version of this figure.*]
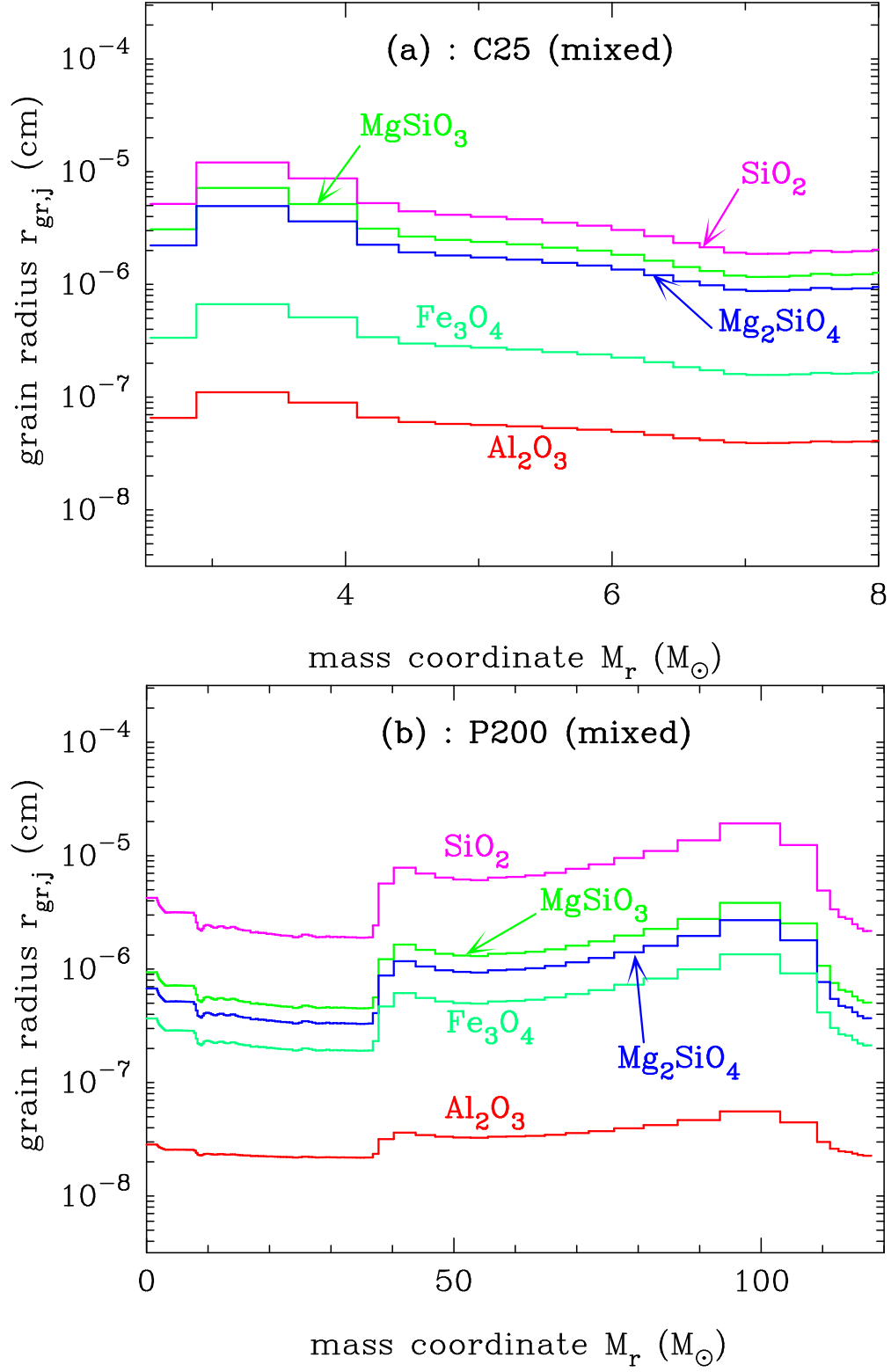
Fig. 10.— The average radii of dust grains formed in the mixed ejecta; (a) for C25 and (b) for P200. [*See the electric edition of the Journal for a color version of this figure.*]
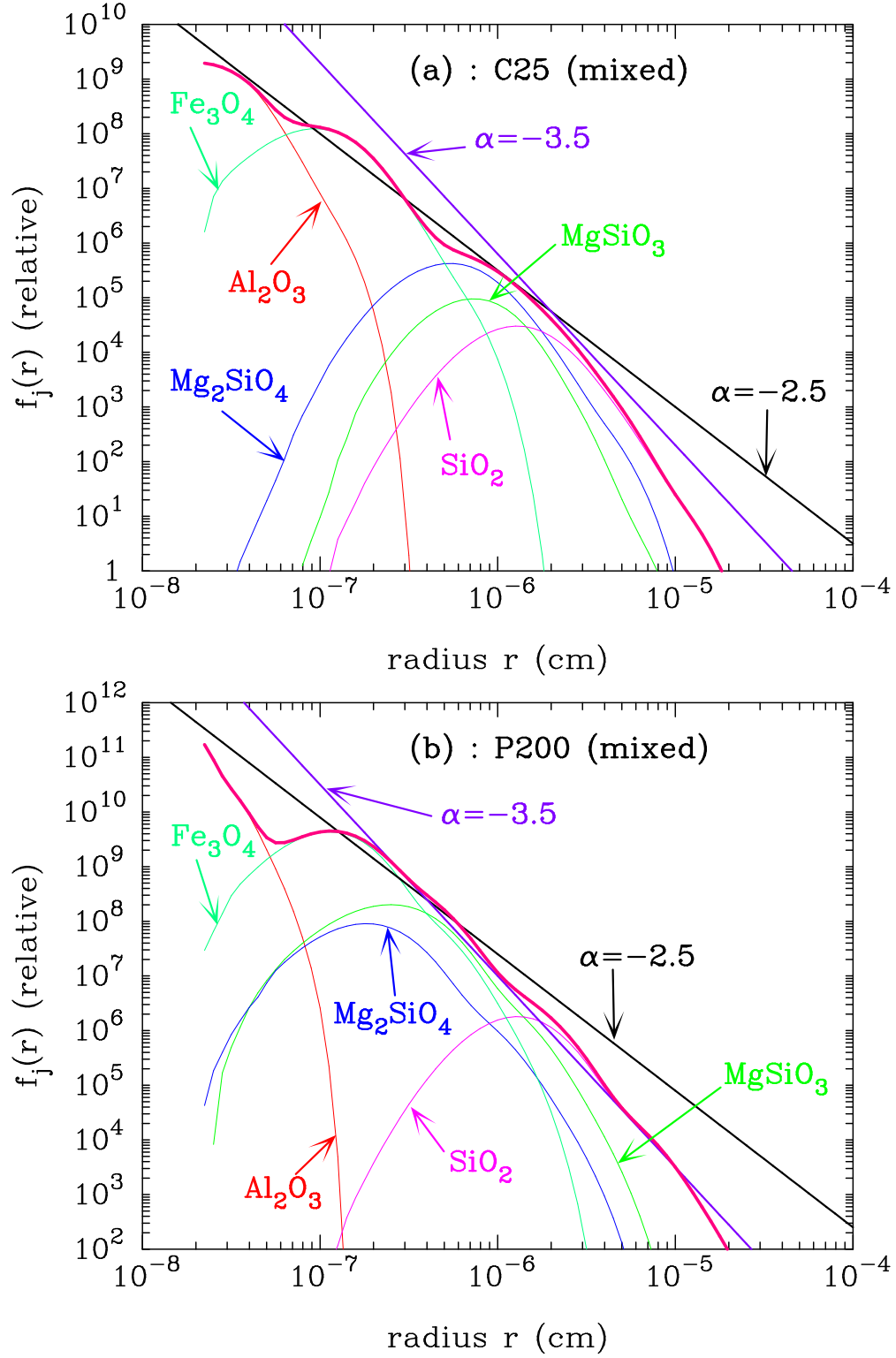
Fig. 11.— The same as Fig. 8 but in the uniformly mixed ejecta; (a) for C25 and (b) for P200. [*See the electric edition of the Journal for a color version of this figure.*]
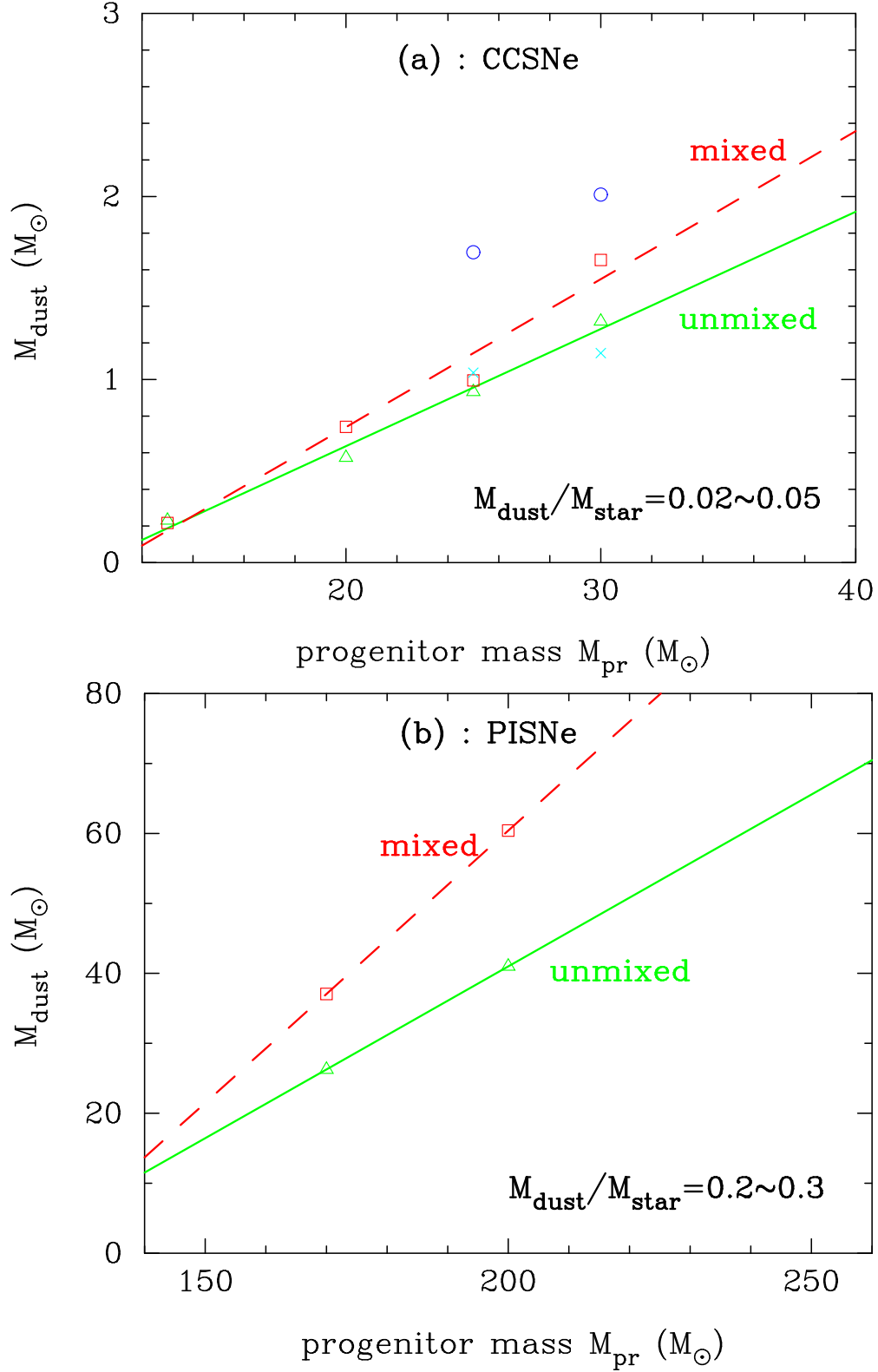
Fig. 12.— The total mass of dust grains formed in the unmixed (open triangles) and mixed (open squares) ejecta of CCSNe and PISNe versus the progenitor mass M_{pr}; (a) for CCSNe and (b) for PISNe. The straight lines indicate the least square's fits to the calculated mass in the unmixed ejecta (solid line) and the mixed ejecta (dashed line) of CCSNe (Fig. 12a), and connect the calculated mass for PISNe (Fig. 12b). Also, in Fig. 12a the total mass of
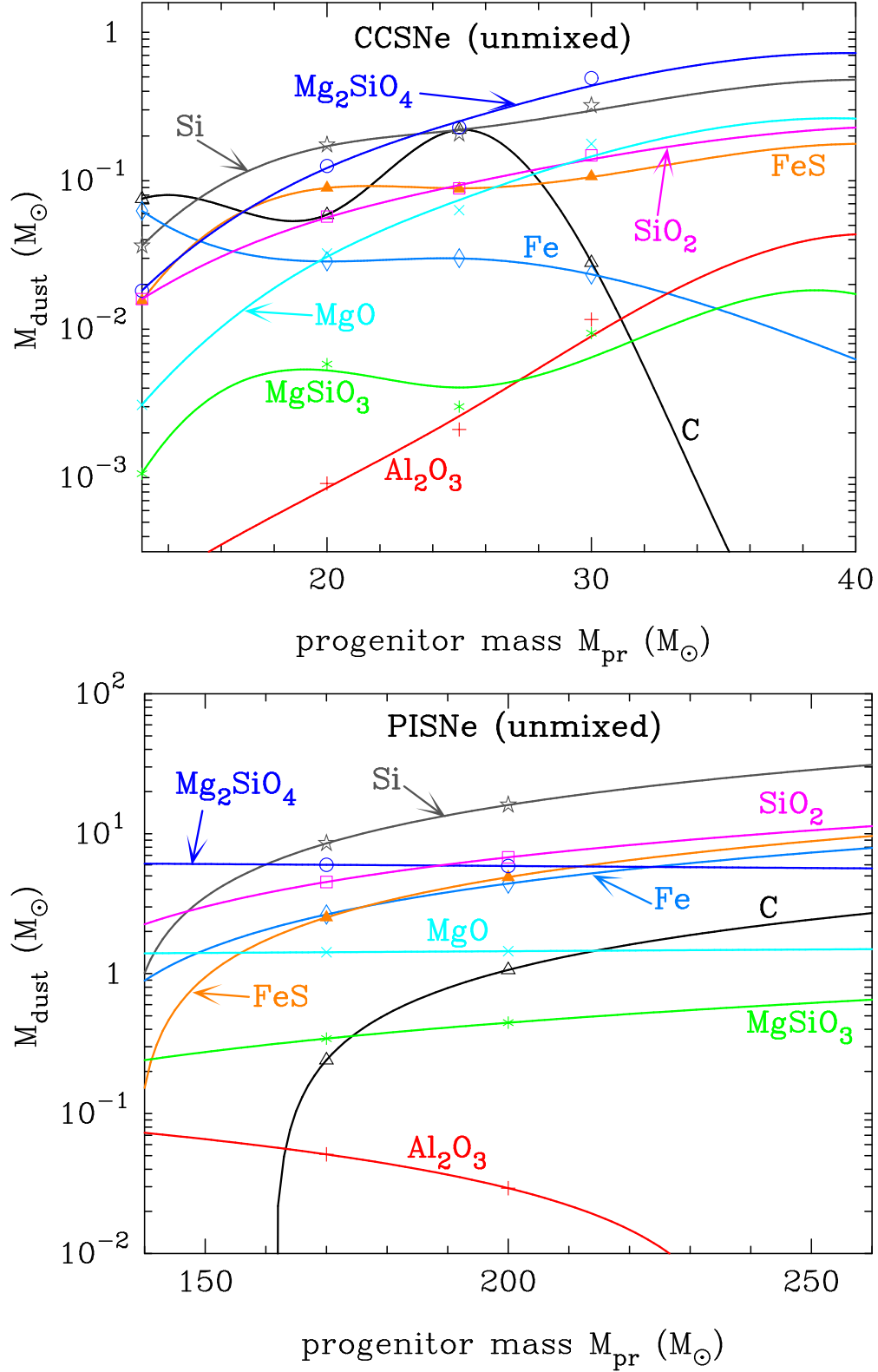
Fig. 13.— The mass yield of each dust grain formed in the unmixed ejecta; (a) for CCSNe and (b) for PISNe. The smooth curves are the least squares' spline fits to the calculated yields for CCSNe (Fig. 13a), and are the straight lines connecting the calculated yields in linear scale for PISNe (Fig. 13b). [*See the electric edition of the Journal for a color version of this figure.*]

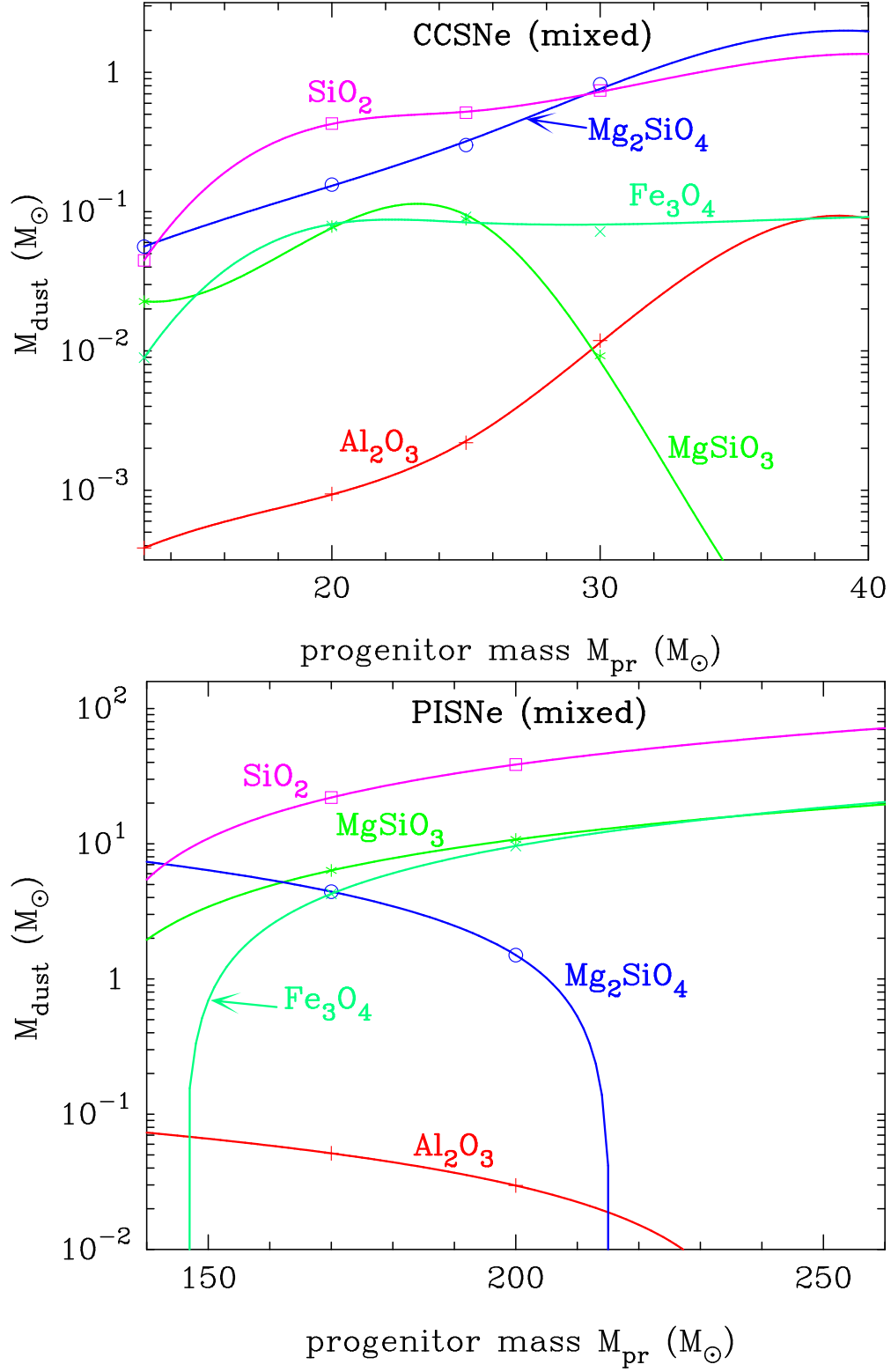Fig. 14.— The same as Fig. 13, but in the mixed ejecta; (a) for CCSNe, and (b) for PISNe. [*See the electric edition of the Journal for a color version of this figure.*]
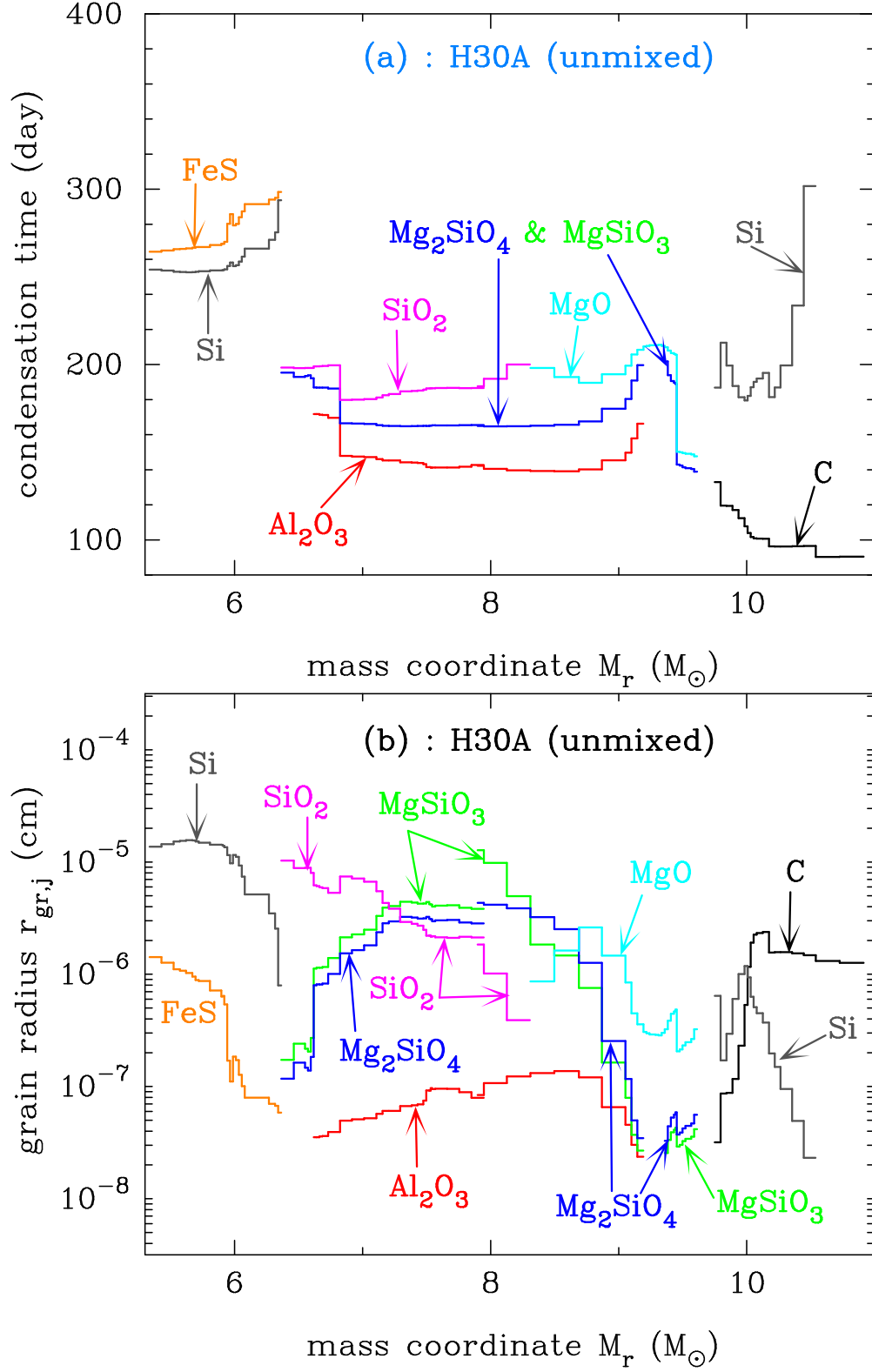
Fig. 15.— The condensation times and the average radii of dust grains formed in the unmixed ejecta of H30A; (a) the condensation times and (b) the average radii. [*See the electric edition of the Journal for a color version of this figure.*]
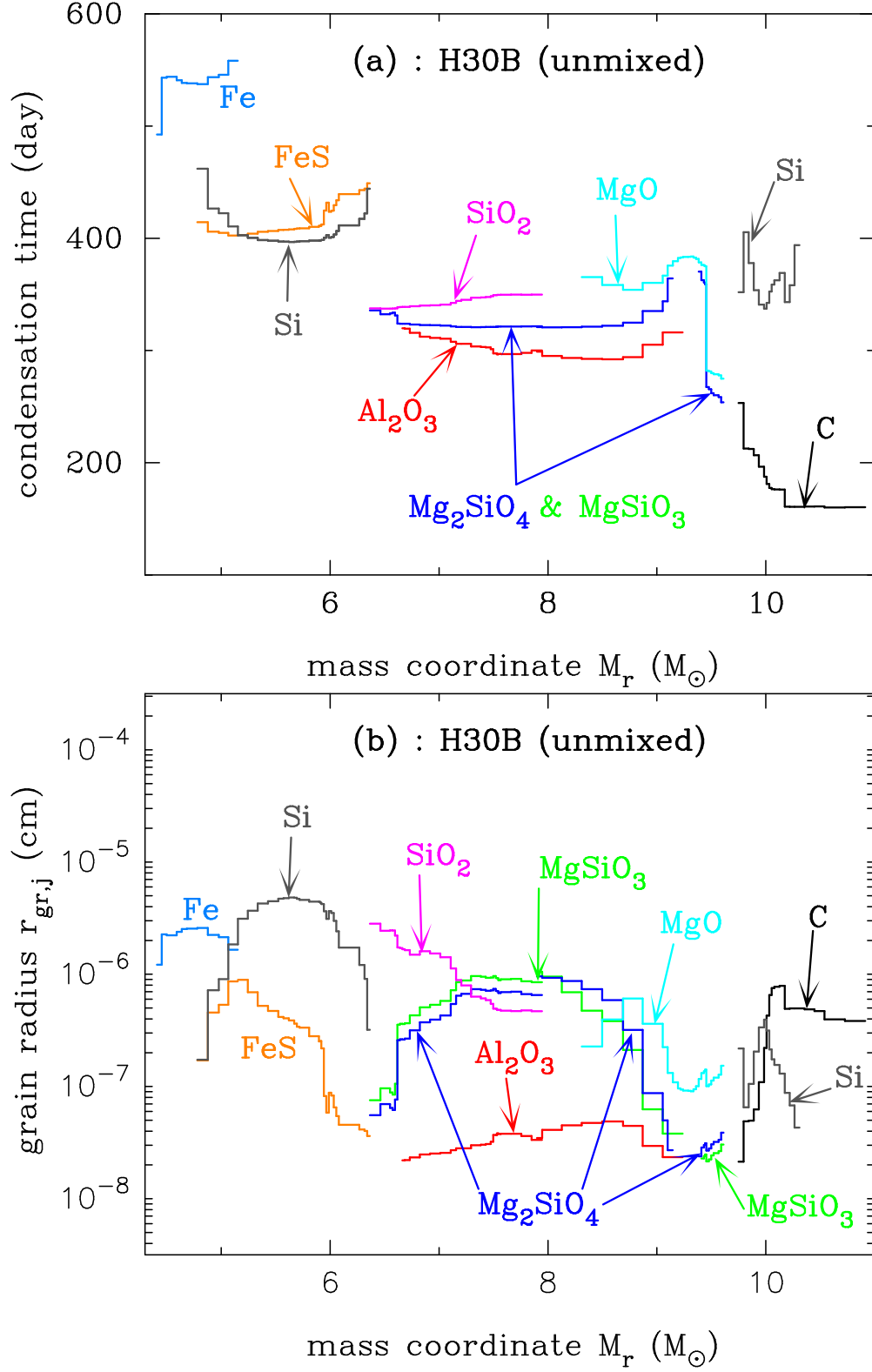
Fig. 16.— The same as Fig 15, but for the unmixed ejecta of H30B. [*See the electric edition of the Journal for a color version of this figure.*]

Fig. 17.— The mass of each grain species versus the mass fraction of carbon f_C and silicon f_{Si} not locked into CO and SiO molecules at $M_r = 3.5\ M_\odot$ in the O–Mg–Si layer of the unmixed ejecta of C20; (a) the mass of each grain species versus f_C where f_{Si} is fixed to 0.9. (b) the mass of each grain species versus f_{Si} with the fixed value of $f_C = 0.99$.

Table 1.   Models of supernovae used in the calculation.

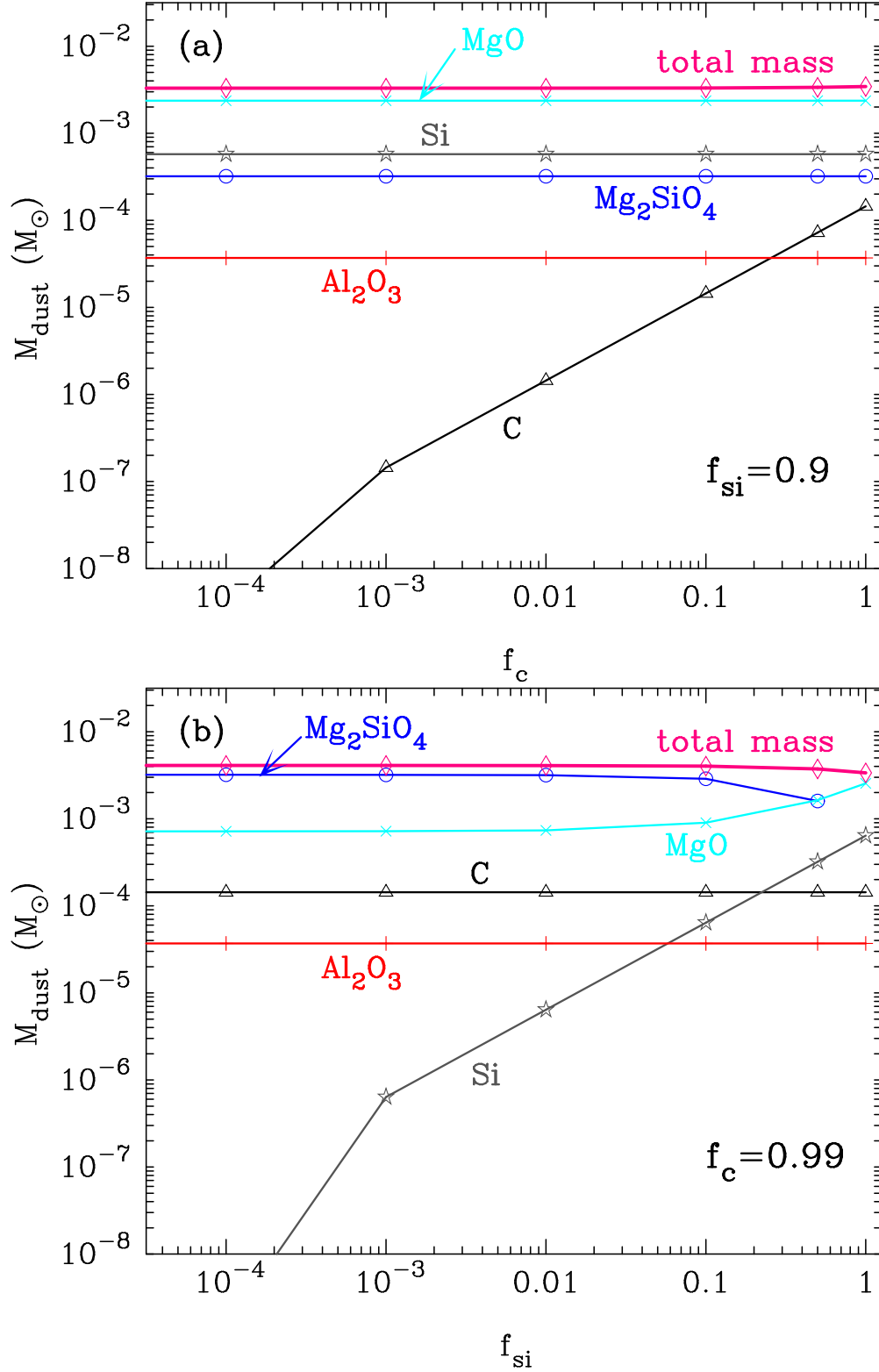| Model	Progenitor mass	Explosion energy	Mass cut	He–core mass	$M(^{56}\text{Ni})$
	$M_\odot$	$E_{51}(10^{51}\text{erg})$	$M_\odot/M_r$	$M_\odot$	$M_\odot$
C13	13	1	1.50	2.05	0.07
C20	20	1	2.45	5.79	0.07
C25	25	1	2.54	8.01	0.07
C30	30	1	2.54	10.7	0.07
P170	170	20	0	82.4	3.56
P200	200	28	0	117.3	7.25
H25A	25	10	3.29	8.01	0.07
H25B	25	10	2.47	8.01	0.7
H30A	30	30	5.31	10.9	0.07
H30B	30	30	4.33	10.9	0.7

Note. — The labels C, P and H of the model represent ordinary CCSNe, PISNe and HNe, respectively, and the numerical value denotes the mass of progenitor in units of solar mass.

Table 2.   Grain species considered in the calculation.

Grains	Key species	Chemical reactions	$A/10^4$(K)	B	σ_j (erg/cm^2)	a_{0j}(Å)
$Fe_{(s)}$	$Fe_{(g)}$	$Fe_{(g)} \rightarrow Fe_{(s)}$	4.84180	16.5566	1800[a]	1.411
$FeS_{(s)}$	$Fe_{(g)}/S_{(g)}$	$Fe_{(g)} + S_{(g)} \rightarrow FeS_{(s)}$	9.31326	30.7771	380[b]	1.932
$Si_{(s)}$	$Si_{(g)}$	$Si_{(g)} \rightarrow Si_{(s)}$	5.36975	17.4349	800[c]	1.684
$Ti_{(s)}$	$Ti_{(g)}$	$Ti_{(g)} \rightarrow Ti_{(s)}$	5.58902	16.6071	1510[c]	1.615
$V_{(s)}$	$V_{(g)}$	$V_{(g)} \rightarrow V_{(s)}$	6.15394	17.8702	1697[c]	1.490
$Cr_{(s)}$	$Cr_{(g)}$	$Cr_{(g)} \rightarrow Cr_{(s)}$	4.67733	16.7596	1880[c]	1.421
$Co_{(s)}$	$Co_{(g)}$	$Co_{(g)} \rightarrow Co_{(s)}$	5.03880	16.8372	1936[c]	1.383
$Ni_{(s)}$	$Ni_{(g)}$	$Ni_{(g)} \rightarrow Ni_{(s)}$	5.09130	17.1559	1924[c]	1.377
$Cu_{(s)}$	$Cu_{(g)}$	$Cu_{(g)} \rightarrow Cu_{(s)}$	3.97955	14.9083	1300[c]	1.412
$C_{(s)}$	$C_{(g)}$	$C_{(g)} \rightarrow C_{(s)}$	8.64726	19.0422	1400[d]	1.281
$SiC_{(s)}$	$Si_{(g)}/C_{(g)}$	$Si_{(g)} + C_{(g)} \rightarrow SiC_{(s)}$	14.8934	37.3825	1800[e]	1.702
$TiC_{(s)}$	$Ti_{(g)}/C_{(g)}$	$Ti_{(g)} + C_{(g)} \rightarrow TiC_{(s)}$	16.4696	37.2301	1242[f]	1.689
$Al_2O_{3(s)}$	$Al_{(g)}$	$2Al_{(g)} + 3O_{(g)} \rightarrow Al_2O_{3(s)}$	18.4788	45.3543	690[g]	1.718
$MgSiO_{3(s)}$	$Mg_{(g)}/SiO_{(g)}$	$Mg_{(g)} + SiO_{(g)} + 2O_{(g)} \rightarrow MgSiO_{3(s)}$	25.0129	72.0015	400[h]	2.319
$Mg_2SiO_{4(s)}$	$Mg_{(g)}$	$2Mg_{(g)} + SiO_{(g)} + 3O_{(g)} \rightarrow Mg_2SiO_{4(s)}$	18.6200	52.4336	436[h]	2.055
	$SiO_{(g)}$		37.2400	104.872		2.589
$SiO_{2(s)}$	$SiO_{(g)}$	$SiO_{(g)} + O_{(g)} \rightarrow SiO_{2(s)}$	12.6028	38.1507	605[g]	2.080
$MgO_{(s)}$	$Mg_{(g)}$	$Mg_{(g)} + O_{(g)} \rightarrow MgO_{(s)}$	11.9237	33.1593	1100[g]	1.646
$Fe_3O_{4(s)}$	$Fe_{(g)}$	$3Fe_{(g)} + 4O_{(g)} \rightarrow Fe_3O_{4(s)}$	13.2889	39.1687	400[g]	1.805
$FeO_{(s)}$	$Fe_{(g)}$	$Fe_{(g)} + O_{(g)} \rightarrow FeO_{(s)}$	11.1290	31.9850	580[g]	1.682

[a]Elliott, Gleiser, & Ramakrishna (1963)

[b]Kozasa & Hasegawa (1988)

[c]Elliott & Gleiser (1960)

[d]Tabak et al. (1975)

[e]Kozasa et al. (1996)

[f]Rhee (1970)

[g]Overbury, Bertrand, & Somorjai (1975)

[h]Boni & Derge (1956)

Note. — The key species is defined as the gaseous species of the least collisional frequency among the reactants. The Gibbs free energy ΔG_j^0 for formation of the condensate from the reactants per the key species is approximated by a formula $\Delta G_j^0/kT = -A/T + B$, and the numerical values A and B are evaluated by least–squares fitting of the thermodynamics data (Chase et al. 1985) in the range of temperatures of interest. σ_j is the surface energy of the condensate, and a_{0j} is the hypothetical radius of the condensate per the key species whose values are calculated from the molar volumes tabulated by Robie & Waldbaum (1968).